DUST IN THE SMALL MAGELLANIC CLOUD

Progress Report

NASA GRANT: NAG 5 14

Period: January 1st, 1992 to October 31st, 1993

Principal Investigator: A. M. Magalhães

Present Address:
Instituto Astronomico e Geofisico
Universidade de São Paulo
Caixa Postal 9638
São Paulo - SP 01065-970
BRAZIL

Phone: 55(11)577-8599, x-231
mario@argus.iagusp.usp.br

DUST IN THE SMALL MAGELLANIC CLOUD

I. SUMMARY OF THE PROPOSAL

Observations of reddened stars in the Small Magellanic Cloud (SMC) indicate that the interstellar grains in that galaxy may show distinct optical properties from those in the Galaxy. In a careful study of three SMC objects, Prevot et al. (1984) have shown that the UV extinction law in the SMC is almost linear with inverse wavelength and the 2200Å feature is generally absent.

The first results of a program to determine the wavelength dependence of the interstellar optical polarization in the SMC (Magalhães et al. 1989, 1993) indicate that highly polarized objects are scarce. Our study has uncovered however several objects with optical polarization greater than around 1%: AZV (= Azzopardi and Vigneau 1982) 126, AZV 211, AZV 221, AZV 398 and AZV 456. The latter two have already had their UV extinction law determined. Our aim was to obtain IUE data and determine the UV extinction law also for AZV 126, AZV211 and AZV 221.

AZV 456, which presents a 'galactic' extinction law, has a 'normal' value for its wavelength of maximum polarization, lmax, while AZV 398, which shows a 'typical' SMC extinction curve, shows a somewhat smaller value for such wavelength. AZV 126, AZV 211 and AZV 221 all present extreme small values of lmax but had not had its extinction curve in the UV determined yet.

We therefore aimed at ultimately determining the extinction law in the direction of these three objects. Such results, in combination with the optical polarization data, have an

important bearing on constraining the composition and size distribution of the interstellar dust in the SMC.

In the last report, we described the images we were able to gather with IUE, their processing and the extinction curves derived from them. In this report, we discuss such extinction curves and the theoretical models we have developed to interpret the SMC extinction and polarization data. Details are presented in an enclosed preprint. We also briefly describe the activities in our ongoing polarimetric program of determining the magnetic field structure of the SMC and the images we have collected at Cerro Tololo Interamerican Observatory during the period of this report. Other activities are also described.

II. RESULTS FROM OUR DUST MODELS FOR THE SMC INTERSTELLAR POLARIZATION AND EXTINCTION DATA

With the IUE extinction data on hand (cf. last report), we have developed software for both calculating the optical properties of a dust ensemble and also to fit dust parameters, such as abundances and size distribution, to an observed curve. We have then used extinction (Lequeux et al. 1984; Prevot et al. 1984; Magalhães et al. 1993; Rodrigues et al. 1993) and polarization (Magalhães et al. 1989; Magalhães et al. 1993; Rodrigues et al. 1993) data in order to constrain models for the SMC dust.

Our approach was to first fit the wavelength dependence of the optical polarization of the objects. This fixed the size distribution and amount of anisotropic particles. We then proceeded to fit the two known types of the SMC extinction curves, the 'typical' SMC

curve and the 'anomalous' (for the SMC), AZV 456 curve, which incidentally has a 'normal' value for the wavelength of maximum polarization.

In the enclosed preprint (Appendix 3), 'Dust in the SMC: Interstellar Polarization and Extinction Data and Dust Models', we discuss in greater detail the fits and several other aspects. Our main conclusions may be summarized as per the following two paragraphs:

Fits to the wavelength dependent polarization data were in general possible for stars with small λ_{max}, the wavelength of maximum polarization. They implied distributions which were narrower and shifted to smaller sizes compared to typical Galactic size distributions. However, stars with normal λ_{max}, which have a narrower polarization curve, could not be adequately fit. This happened for any of the dust models employed.

The extinction curves were not equally fit by the different models. The best fits were obtained assuming both a power law size distribution and continuity in the *volume* distribution from the smaller spheres to the larger cylinders, the cylindrical population being taken from the fit to the polarization. The 'typical', monotonic SMC extinction curve could be well fit with graphite and silicate grains and using a small fraction of the SMC carbon locked up in the grains. Amorphous carbon and silicate grains also fit the data well. However, AZV 456, with its Galactic extinction curve, has an UV bump which is too blue to be fit by spherical graphite grains.

III. INTERSTELLAR POLARIZATION IN THE SMALL MAGELLANIC CLOUD

Optical polarization of stars belonging to the SMC carries an important information about the orientation of the interstellar magnetic field in that galaxy. Also, the wavelength dependence of the polarization of the more highly polarized stars provides, as mentioned above, clues as to the nature of the interstellar grains themselves.

Until recently, our polarimetric survey (Magalhães et al. 1990), which provided the targets for this IUE project, has been pursued with photoeletric equipment and by seclecting reddened, early-type stars. As described in the previous report, we had successfully modified the CCD camera at CTIO, Chile, to include a rotating halfwave plate and a calcite block. In this manner, we can now employ an imaging polarimetry technique and its inherent advantage of gathering data on several stars simultaneously. Our initial, engineering run in December 1991 at Cerro Tololo was a success; with our technique, imaging polarimetry can now be performed to a very high, unprecedented even, degree of accuracy.

We have been awarded telescope time specifically for this project during November 1992 and October 1993 and obtained imaging polarimetry of a number of fields in the SMC NE and Wing sections. These areas are of particular interest due to the possible past interaction of the SMC with the LMC and which may have affected these regions. In Fig. 1, we illustrate the positions over the SMC where we have thus far obtained data. The area around each position is about 8'x8'.

We have developed software to obtain the linear polarization of the objects in each field, using photometric software under the IRAF package. We are still developing

additional software in order to automatize the reduction and allow for the determination of the polarization of all stars in each field.

IV. VISITS PAID

In the early summer of 1992, from May 27 to June 26, we paid a planned, month long visit to Dr. George Coyne, at the Specola Vaticana, a co-investigator in this project. We were then able to work towards the IUE data analysis and the preparation of the enclosed preprint.

During that period, we took the opportunity to attend the European Meeting 'New Aspects in Magellanic Cloud Research', where we presented a poster paper (Magalhães 1993). A copy of the paper is enclosed (Appendix 1).

V. PAPERS IN PREPARATION

We are finishing another paper on this project and which is a companion paper to the enclosed preprint. It describes in detail the optical polarimetry and IUE extinction data that served as a basis for this preprint.

VI. M.Sc. THESIS

In October 1992, Claudia Rodrigues, one of the co-investigators in this project, presented her M.Sc. dissertation, 'Interstellar Dust in the Small Magellanic Cloud'

(Rodrigues 1992). At the Astronomy Department, this type of dissertation must always contain original, publishable research and is a mandatory step toward the PhD degree.

The advisor was this project's P.I., A.M. Magalhães. Its English abstract is enclosed (Appendix 2) and a copy of the full dissertation is available.

REFERENCES

Azzopardi, M. and Vigneau 1982, Astron.Ástrophys.Suppl.Ser. **50**, 291.

Lequeux, J., Maurice, E., Prevot, L., Prevot-Burnichon, M. and Rocca-Volmerange, B. 1984, Astron.Astrophys. **113**, L5.

Magalhães, A.M. 1993, in 'New Aspects of Magellanic Cloud Research', B. Baschek, G. Klare and J. Lequeux eds. (Springer: New York), p. 276.

Magalhães, A.M., Piirola, V., Coyne, G.V. and Rodrigues, C.V. 1989, in 'Interstellar Dust Contributed Papers', eds. A.G.G.M. Tielens and L.J. Allamandola, NASA CP-3036.

Magalhães, A.M., Loiseau, N., Rodrigues, C. and Piirola, V. 1990, IAU Symp. 140, p.255.

Magalhães, A.M., Rodrigues, C., Coyne, G. and Piirola, V. 1993, in preparation.

Prevot, M.L., Lequeux, J., Maurice, E., Prevot, L. and Rocca-Volmerange, B. 1984, Astron.Astrophys. **132**, 389.

Rodrigues, C.V. 1992, MSc Dissertation, Departamento de Astronomia, Instituto Astronômico e Geofísico, Universidade de São Paulo.

Rodrigues, C. V., Magalhães, A.M. and Coyne, G.V. 1993, enclosed preprint.

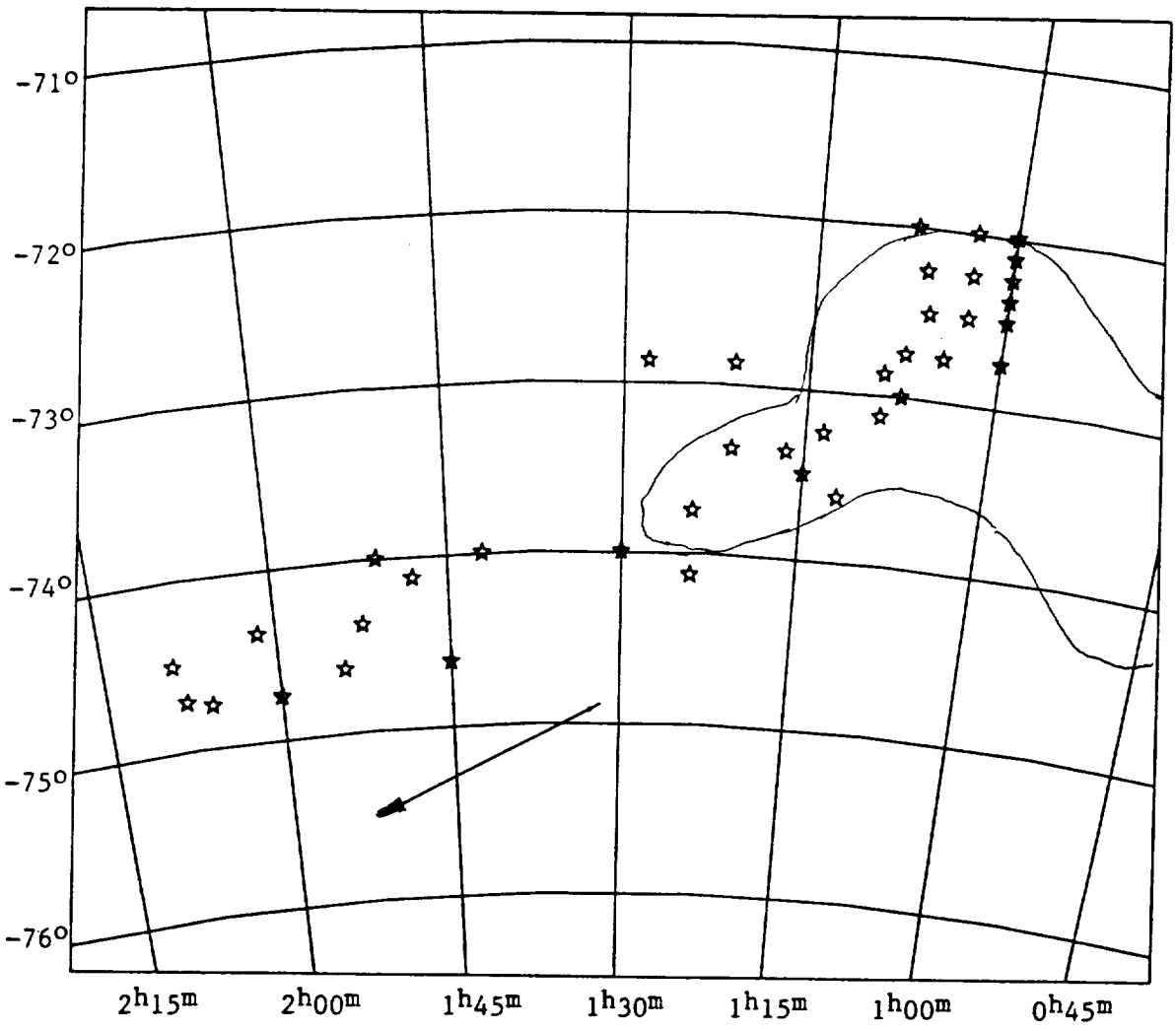

Figure 1. A map in equatorial coordinates of the regions in the SMC where we have obtained CCD imaging polarimetry. Each region is about 8'x8' and for each of these a total of four exposures, with different positions of the waveplate retarder, was obtained. The SMC main body is outlined. The LMC is towards the lower left, in the direction of the arrow. The images will allow a determination of the interstellar magnetic field structure of the SMC in this region of interaction between these two galaxies.

APPENDIX 1

Paper presented at the European meeting 'New Aspects of Magellanic Cloud Research', Heidelberg, June 15-17, 1992 (Magalhães 1993). The meeting happened during the period the PI was paying a visit, within this project, to the co-I. Dr. G. Coyne, at the Vatican Observatory.

THE ENVELOPES OF B[e] SUPERGIANTS IN THE MAGELLANIC CLOUDS

Antonio Mário Magalhães

Space Astronomy Laboratory, U. Wisconsin, Madison, WI 53705, USA
and
Instituto Astronômico e Geofísico, Universidade de São Paulo, Caixa Postal 9638, São Paulo, SP 01065-970, BRAZIL [1]

Abstract: We have obtained linear polarization data of B[e] supergiants in the Magellanic Clouds. Our analysis shows that they have non-spherically symmetric envelopes, with a range of intrinsic polarizations. Comparison of our data with spectroscopic data in the literature agrees with this interpretation. The polarization correlates best with the IR excess due to dust, suggesting dust scattering as the main polarizing mechanism. Comparison of our data with data uncovered from the literature for four stars indicate that the envelopes are stable.

Introduction

The B[e] supergiants populate the hot, luminous part of the H-R diagram, together with the Luminous Blue Variables and the Wolf-Rayet stars. While there is evidence that the LBV are progenitors of WR stars, the relation of B[e] stars to these classes and to the evolution of massive stars is not clear. Spectra of B[e] stars suggest (Zickgraf 1990) a hot, fast, radiatively driven polar wind together with a slow, dense, cool equatorial flow; in other words, their envelope could be very far from spherical symmetry. Non-spherically symmetric envelopes linearly polarize starlight. If measurable, polarization would hence potentially carry information on the B[e] star environment.

Observations

Optical linear polarization data have been obtained with the VATPOL polarimeter (Magalhães et al. 1984), at the 2.15m telescope at the CASLEO observatory, San Juan, Argentina. The data has been corrected for foreground (Galactic plus Magellanic) interstellar polarization (for details, see Magalhães 1992).

[1] Present address

Results

The main results may be summarized as follows:

a. Significant polarization has been detected in most of the objects. The B[e] star envelopes are hence notably non-spherically symmetric. Modelling shows that the histogram of observed polarizations is consistent with the Magellanic B[e] stars having a *distribution* of intrinsic polarizations.

b. The observed polarizations do not correlate to any statistically significant level with the near IR excess from the free-free radiation from the B[e] star envelopes. However, the observed polarizations do correlate significantly with the IR excess at longer wavelengths, due to dust, which forms in the outer parts of the B[e] star envelopes.

c.Data has been recovered from interestellar polarization surveys for 4 B[e] stars. A comparison with our data shows no statistical evidence for variability; this indicates that the envelopes are stable. More observations to stablish this on a firmer basis are still needed.

The full analysis and results are being published elsewhere (Magalhães 1992). They will include a discussion between the data and the detection of CO emission from the Magellanic B[e] stars and also a comparison with polarimetric data of Galactic B[e] stars.

Acknowledgements. This research has received support from grants by NASA (NAS5- 26777) and São Paulo state funding agency FAPESP (89/1670-9). His attending this meeting was supported by the Vatican Observatory and NASA grant NAG5-1463.

References

Magalhães, A.M. (1992): ApJ, 10 October, in press
Magalhães,A.M., Benedetti, E. and Roland, E.W. (1984): PASP **96**, 383
Zickgraf, F.-J. (1990): in "Angular Momentum and Mass Loss for Hot Stars", ed. by L.A. Willson and R. Stalio (Dordrecht: Kluwer), 245

APPENDIX 2

Frontspiece and abstract of the MSc dissertation of Claudia Rodrigues, one of the co-I's, presented in October 1992.

USP INSTITUTO ASTRONÔMICO E GEOFÍSICO

POEIRA INTERESTELAR
NA
PEQUENA NUVEM DE MAGALHÃES

Cláudia Vilega Rodrigues

DISSERTAÇÃO DE MESTRADO
Departamento de Astronomia
Orient.: Dr. Antonio Mário Magalhães
- 1992 -

SÃO PAULO - BRASIL

ABSTRACT

We have studied the interstellar dust in the Small Magellanic Cloud employing visible polarimetry and ultraviolet spectrophotometry. The SMC typical extinction curve is not fitted by the standard grain model that uses a power law size distribution of bare grains. We suggest some modifications in order to best fit the data. Only one star presents the 2175Å bump in the extinction. It seems to be shifted to bluer wavelengths with relation to its mean Galactic value, which cannot be reproduced by spherical graphite grains.

The analysis of the polarimetric data by the most popular grain models indicates that the grains seem to be generally smaller in the SMC than in the Milky Way Galaxy. However, some stars show the wavelength of the maximum polarization, λ_{max}, at wavelengths similar to the Galaxy, albeit with a distinct relation between the curve width and λ_{max}. The polarization curves of such stars are not well fitted by the grain models. In addition, there is a possible correlation between the spectral dependence of the polarization and that of the extinction curve, in sense that stars with smaller λ_{max} do not present the 2175Å bump.

APPENDIX 3

Preprint with the SMC dust model results. Another preprint, with the full set of observational (IUE and ground based) data, is in preparation.

DUST IN THE SMC: INTERSTELLAR POLARIZATION AND EXTINCTION DATA AND DUST MODELS

C. V. Rodrigues[1], A. M. Magalhães[1] and G. V. Coyne, S.J.[2]

Received: _____; Accepted: _____

ABSTRACT

We study the dust in the Small Magellanic Cloud using available polarization and extinction data and popular dust models. Such data suggest that the monotonic SMC extinction curve is associated with values of λ_{max}, the wavelength of maximum polarization, smaller than the Galactic average. On the other hand, AZV 456, a star with an extinction similar to the Galactic one, shows also a normal λ_{max}.

Fits to the wavelength dependent polarization data were possible for stars with small

---

[1] Instituto Astronômico e Geofísico , Universidade de São Paulo, Caixa Postal 9638 - 01065 970 São Paulo - SP

[2] Vatican Observatory

λ_{max}. They, in general, implied distributions which are narrower and shifted to smaller sizes compared to typical Galactic size distributions. However, stars with normal λ_{max}, which have a narrower polarization curve, could not be adequately fit. The use of narrow size distribution seems did not improve the results. This was valid for any of dust models used.

The extinction curves were not equally fit by the different models. The best fits were obtained with a power law size distribution. Also, the best fits were obtained assuming that the cylindrical and spherical silicate grains have a size distribution in which the *volume* distribution from the smaller spheres to the larger cylinders was continuous, taking the cylindrical population from the fit to the polarization. The 'typical', monotonic SMC extinction curve could be well fit with graphite and silicate grains and using a small fraction of the SMC carbon locked up in the grains. Amorphous carbon and silicate grains also fit the data well. However, AZV 456, with its Galactic extinction curve, has an UV bump which is too blue to be fit by spherical graphite grains.

Subject Headings: ISM: dust, extinction - polarization - ultraviolet: interstellar - galaxies: Magellanic Clouds

1. INTRODUCTION

Most presently favored grain models assume the interstellar grains as formed by silicates in an amorphous form and carbon, probably in the form of graphite. Mathis, Rumpl & Nordsieck (1977, hereafter MRN) suggested homogeneous grains of silicate and graphite with a power law size distribution. A model considering the grains within an evolutionary context is advocated by Greenberg and collaborators (e.g., Hong & Greenberg 1980; Chlewicki & Greenberg 1990). In this case, the bigger grains are assumed as a silicate nucleus recovered by an organic refractory material and the smaller ones are homogeneous silicate and graphite grains. In the model of Duley, Jones & Williams (1989, hereafter DWJ), the grains are silicate nuclei covered with a hydrogenated amorphous carbon mantle. Contrary to the former models, where the 2175 Å bump is produced by a graphite grain population, in the DWJ model the bump is produced by electronic transitions in OH- ions within small silicate grains (Duley 1987).

The Magellanic Clouds are the nearest external galaxies. The Small Magellanic Cloud (SMC) is characterized by a small dust content which makes any study of its dust component difficult. The most reddened stars have a color excess of less than 0.40^{mag} (Bouchet et al. 1985). Galactic foreground extinction has a maximum value of 0.09^{mag} (Schwering 1988). The infrared (IR) extinction is similar to that of the Galaxy, with a slightly smaller value of R ($=A_V/E_{B-V}$) of 2.7 (Bouchet et al. 1985). In contrast, the UV extinction is very different from either the Galaxy or the LMC. It is roughly linear up to 9 μm^{-1} and does not show the 2175 Å bump (Prevot et al. 1984). The SMC average gas-to-

dust ratio (N(H)/E(B-V)) is about 10 times the Galactic (Bouchet et al. 1985), consistent with its smaller metallicity (e.g., Wheeler, Sneden & Truran 1989 and references therein).

Interestingly however, the SMC star AZV456 (AZV = Azzopardi & Vigneau 1982) has its line of sight characterized by an extinction similar to the average in the Galaxy and with a Galactic gas-to-dust ratio (Lequeux et al. 1984). Its interstellar lines have SMC typical velocities which discards the possibility of a foreground Galactic extinction (Lequeux et al. 1984; Martin, Maurice & Lequeux 1989). There is an SMC IR extended source located at exactly the same coordinates (LI-SMC 140: Schwering & Israel 1990), which supports an extinction of Magellanic origin.

The SMC IR emission was studied by Sauvage, Thuan & Vigroux (1990) using IRAS data. They concluded that the small 12 μm emission is associated with a smaller number of very small grains (macromolecules) compared to the large ones. They attributed this to the low SMC metallicity. To explain the SMC 25 μm emission, Sauvage et al. (1990) postulated the existence of a thermalized grain population of intermediate size between the very small and the big grains. The only work concerning IR spectroscopy in the SMC was made by Roche, Aitken & Smith (1987). They did not detected the 9.7 μm silicate band in an compact HII region. However, this is an isolate result that could not represent the SMC interstellar medium (ISM) as a whole.

Bromage & Nandy (1983) and Pei (1992) have studied the SMC 'typical' extinction curve using the MRN model, with only spherical particles. They concluded that the simple reduction of the quantity of graphite grains relative to the silicate ones in the Galactic models allows the reproduction of the SMC extinction, without changes in the sizes used

to obtain the Galactic curve.

The scope of this work is study the physical properties of the dust in the SMC in light of existing dust models. We use *both* extinction and polarization data (Lequeux et al. 1984; Prevot et al. 1984; Magalhães et al. 1993) in order to constrain the models' parameters. In the next section, we briefly describe the models and their application to the average Galactic extinction and polarization curves. We then present the fits to wavelength dependence of the SMC polarization and extinction as well as a discussion about the importance of the changes in the parameters and the needed elemental abundances in the third section. We summarize the main results in the final section.

2. DESCRIPTION OF THE MODELS

The theoretical calculation of the interstellar extinction and polarization consists basically of an average of the extinction cross sections of grains of different sizes weighted by the size distribution (e.g., Greenberg 1968) since the multiple scattering is not important. The polarization is the result of a differential extinction in the two directions perpendicular to the line of sight. This effect can be achieved by anisotropies in the shape and/or in the optical properties of the grain. A model must thus define the size distribution as well as the optical and morphological properties of the grains.

The size distribution, $n(a)$, can be algebraically represented as

$$n(a) = K f(a), \qquad (1)$$

where a is the particle radius, $f(a)$ describes the shape of the size distribution, and K is related to the absolute number of grains. This constant will be hereafter called the normalization constant, which is dependent on the elemental abundance (gas + solid phase) and depletion of the main grain constituents. Here we have used the word depletion defined as the fraction of a given element locked up in the grains. The abundances of interest are usually those of carbon (C) and silicon (Si). The calculation of the wavelength dependence of the polarization requires an assumed $f(a)$, i.e., the shape of the size distribution. The normalization constant, K, does not need to be specified. The extinction is usually calculated taking into account more than one grain population. Hence, we must know not only the form of each size distribution but also the relative number of grains of each species in order to calculate their contribution to the total extinction curve.

In this work, we have considered two shapes for the grain particles: spheres and cylinders. The latter were assumed as a good approximation to elongated particles. The cross sections of spherical particles have been calculated using Mie's theory (e.g., Bohren & Huffman 1983), while the infinite cylinder cross sections were calculated using the formulae in Lind & Greenberg (1966) for homogeneous grains and in Shah (1970) for coated grains. Those cross sections represent well finite cylinders and are not qualitatively too different from spheroids (e.g., Wolff, Clayton & Meade 1993).

The elongated particles must be aligned to produce the polarization, otherwise the net effect is of an isotropic medium. This alignment is commonly considered as being produced by the paramagnetic relaxation mechanism arisen from an imaginary part of the magnetic susceptibility which tends to make the grain spins with its angular momentum parallel to the magnetic field, but perpendicular to the major axis of the grain (Davis &

Greenstein 1951). Hildebrand (1988) has reviewed this and other alignment mechanisms and their eventual difficults. The degree of alignment can be described by a number distribution of grains that have a given angle between their angular momenta and the magnetic field; the highest its efficiency, the larger the number of grains having their angular momenta parallel to the magnetic field. This case is usually called partial alignment. We have assumed the perfect alignment hypotheses, i.e., all the grains having their angular momentum perfectly parallel to the magnetic field. This approximation seems not to produce important differences relative to the partial alignment situation (Chlewicki & Greenberg 1990 - Fig. 1b), at least with respect to the spectral dependence of the polarization. In this scenario, the angle between the magnetic field and the plane of sky, γ, must be specified.

We have considered different grain compositions. Three kinds of silicates have been used. The optical properties of one of them has been taken from Draine & Lee (1984), a synthesis of laboratory and astronomical data; it is commonly called *astronomical silicate*. Its properties are quite similar to the olivine ($[Mg,Fe]_2SiO_4$), possessing the inflexion around 6.5 μm^{-1} characteristic of that material. We have also used the optical constants of enstatite ($[Mg,Fe]SiO_3$) obtained by Huffman & Stapp (1971). This material was employed by Bromage & Nandy (1983) in their fit of the SMC typical extinction curve and has, in contrast to astronomical silicate, a steeper monotonic UV extinction. Basaltic glass (Pollack, Toon & Khare 1973; Lamy 1978) was employed in the DWJ polarization model. The index of refraction of graphite has been also taken from Draine & Lee (1984). The "1/3-2/3" approximation was used. Amorphous carbon was also considered here, using the constants of Duley (1984). The dielectric material properties in Greenberg's grain mantle is from Chlewicki & Greenberg (1990).

We now discuss in detail the influence of different parameters in the context of the different grain models. While general, the discussion has an emphasis on those that will have a bearing on the interpretation of the SMC data.

2.1. MRN Model

2.1.1. Extinction Parameters

The MRN model considers the grains as being homogeneous particles of silicate and graphite with a power law size distribution of index -3.5. The size ranges are 0.02 and 0.25 μm for silicate grains and 0.005 and 0.25 μm for graphite grains. Mathis et al. (1977) proposed a model only with spherical particles. However, Mathis (1979, 1986) discussed a complementary population of elongated grains (cylinders) in order to produce the polarization. A single size distribution described both silicate populations. From a minimum grain radius, a^{sil}_{-}, until an intermediate radius, a^{sil}_{p}, the grains were assumed to be spherical (or not aligned), and from them on until a maximum radius, a^{sil}_{+}, they were taken as aligned cylinders. Plots of the extinction where part of the spherical silicates are replaced by cylindrical particles, in spite of the possible differences in the extinction produced by the different shapes, have apparently not been presented. In Fig. 1, we have plotted extinction curves using spherical silicates only and also silicates both as spherical and cylindrical grains. The points represent the average Galactic extinction curve of Savage & Mathis (1979). The Galactic abundances have been extracted from the data of Anders & Grevesse (1989). The C depletion was assumed to be 60% (i.e., 60% of the carbon is in form of grains) according to Draine & Lee (1984). The minimum cylinder size

used was 0.055 μm as opposed to 0.08 μm in Mathis (1979). That range size could not produce a Galactic polarization curve, probably because the distinct indexes of refraction. Overall, the result using also cylinders is quite distinct from that obtained by using only spheres. It is seen that the visible extinction produced by silicates and cylinders is smaller than that produced only by spheres in such way that the contribution of graphite must be enlarged in order to produce the same amount of extinction. This makes the level of the FUV be smaller, since the extinction of the small silicate spheres has a reduced weight. In the IR, the value of R is practically twice the observed. Obviously, the spherical model is an approximation that can only supply partial information about the grains in a given line of sight.

If only spherical grains are considered, only the carbon and silicate abundances and their depletions must be specified. However, in the case of having the silicate grains in two morphologically distinct populations, the elemental fraction used by each silicate population must also be known. In the single size distribution (when silicate cylinders and spheres have the same normalization constant) of Mathis (1979), these fractions are automatically fixed by one boundary condition: the number of cylinders and spheres at the radius a^{sil}_p must be the same. Hereinafter, we call this case of *size continuity*. In addition, we have here also studied another kind of continuity between the two silicate populations. We employ the same shape, $f(a)$, for both populations. The normalization constant, K, however, was not assumed to be the same for cylinders and spheres. Specifically, we have calculated these in such a way that the **volume** distribution is continuous, i.e., the boundary condition is such that the volume of spherical and cylindrical grains of size a^{sil}_p must be equal. This will be called *volume continuity*. Let two particles be of same radius but with one spherical and another cylindrical. The latter has a greater volume; a larger

number of spherical particles will be then necessary in order to have the same total volume occupied by the elongated particles. The normalization constant of the silicate spheres is hence larger than the one of the cylindrical particles. This results in a large relative contribution by spherical particles in the case of the *volume* continuity. Consequently, the FUV is more enhanced in the latter case (Fig. 2). It can be seen that the IR portion of the extinction curve is not much altered, only the UV is changed as a consequence of a more enhanced extinction from the small silicate spheres in the case of *volume* continuity.

The strong absorption seen in the Galactic extinction around 2200 Å curve can be reproduced by the graphite and most models considered it as the carrier. This is well reviewed by Draine (1989). If the abundances are maintained fixed, the changes in the C depletion are reflected by different contributions of the graphite extinction to the total curve. Obviously, the increase of the C depletion is reflected in a stronger bump. In the IR, the contribution of the graphite grains is small so R decreases when the C depletion increase. The graphite extinction is responsible by the FUV curvature in the MRN model, so it also increases with a larger depletion.

As will be seen later in the fits of the SMC extinction, astronomical silicate and enstatite have distinct UV behavior. Enstatite, roughly speaking, simulates astronomical silicates of smaller sizes, since the extinction in the blue is enhanced, while smaller in the IR. This effect is also true for the polarization (see also Fig. 7 below). The FUV curvature produced by graphite masks the saturation by the astronomical silicate around 6.5 μm, that will be clear in the SMC plots.

Another parameter of the extinction curve is the angle between the magnetic field and the

plane of sky, γ, that defines the alignment of the elongated grains. The extinction curve is pratically not sensitive to this parameter. The small differences that appear are such that smaller angles simulate larger grain sizes (Hong and Greenberg 1980 and references therein). Larger changes, however, are seen in the polarization. We use cylinder sizes that fit the average Galactic polarization curve with $\gamma = 60^{o}$. Hence, the polarization produced using other values of γ will be different from the average Galactic curve, but here our intention is only to illustrate the effects of varying γ on the extinction curve.

Next, we discuss the influences of the size distribution parameters in the extinction curve. The extinction produced by a silicate distribution extended for smaller a^{sil}_{-} has an enhanced FUV extinction, since there are more grains contributing to the extinction towards smaller wavelengths. The slope of the extinction after 6.5 μm increases a bit with a^{sil}_{-}. In the MRN model, the maximum size of spherical silicates, a^{sil}_{p}, is the same of the minimum cylindrical silicates, in such way that, the variation of this parameter has two effects. When the spherical silicate population is extended to larger sizes, the FUV extinction of the spheres is larger. Secondly, when the minimum size of the cylindrical population increases, the saturation of the extinction caused by this population occurs at larger wavelengths and at a smaller level. We have, hence, changes in the level and shape of the extinction produced by the silicates, mainly in the curvature in the FUV. Fig. 3 shows that the curvatures are smoother for smaller a^{sil}_{p}. The modifications in the maximum size of the cylindrical population, a^{sil}_{+}, affect mostly the visible, the region of the normalization, so the extinction changes throughout the spectra but it is more accentuated in the extremes. The level of the FUV extinction is greater for smaller sizes, and the shape in the IR and visible changes in such way that greater values of R are obtained for greater sizes (Fig. 4).

The changes in the parameters of graphite population are mainly reflected in the bump extinction (Fig. 5). Its position is more sensitive to changes in the minimum size of graphite grains, a^{gr}_{-}, which increases to bumps located at redder wavelengths. The increase of a^{gr}_{-} also makes the bump slight stronger. The increase of a^{gr}_{+}, the maximum size of graphite, produces bumps more shallow and also the FUV extinction is sligthly reduced. The IR extinction has a small increase for large a^{gr}_{+}.

2.1.2. Polarization Parameters

There are two approaches to the polarization within the MRN model context. Mathis (1979) proposed a simple replacement of a part of the spherical grains by cylindrical ones (as described above). This case will be called MRN model. Mathis (1986, hereafter M86) proposed a modification in the above scenario. The polarizing material would consist of silicate particles containing inclusions of ferromagnetic material in order to make the alignment more efficient (Jones & Spitzer 1967). The number of these inclusions increases with the grain size in such a way that larger grains have greater probability of been aligned. This probability is given by

$$p(a) = 1 - exp\left\{-\left(\frac{a}{a'}\right)^3\right\} \qquad (2)$$

where a' is the smaller size containing a superparamagnetic incursion. In order to reproduce the K x λ_{max} relation of Wilking et al. (1980), its dependence with λ_{max} is given by

$$a' = 0.329\,\lambda_{max}^{2.17}\,. \qquad (3)$$

Hence, a' is fixed by the observed λ_{max}. As the grains need to be aligned to produce the polarization, the effective number of grains contributing to polarization is given by the size distribution multiplied by the above probability.

A polarization model involves relatively few parameters: the maximum and minimum cylinder sizes, $a^{sil}{}_p$ and $a^{sil}{}_+$, respectively, and the direction of the magnetic field, γ. For small values of γ, i.e., when the magnetic field has a large component perpendicular to the line of sight, the polarizing efficiency of the grains increases, and the polarization curve becomes narrower (Hong & Greenberg 1980). It can be also noted that λ_{max} shifts to bluer wavelength, simulating smaller grains. Decreasing $a^{sil}{}_p$, λ_{max} has a noticeable shift to bluer wavelength and the whole curve is modified (Fig. 6). On the other hand, when $a^{sil}{}_+$ is changed, only the "red" part of the polarization curve is altered (Fig. 6), because the remainder of the curve is produced by the more numerous smaller grains. As with the extinction, enstatite results in a extinction corresponding to smaller grains as compared to astronomical silicate (Fig. 7).

The fits using M86 produce a polarization curve with the maximum towards redder wavelengths as compared to the MRN model, because the value of a' of 0.09 μm (supposing a λ_{max} of 0.55 μm). Hence only the large grains are contributing to the polarization. It is important to note that it is not possible to change this curve modifying $a^{sil}{}_-$; a' and $a^{sil}{}_p$ are the important parameter in fitting a given polarization curve.

2.2. Greenberg's model

In Greenberg's model (e.g., Hong & Greenberg 1980), the large grains are considered to be formed by nucleus of silicate recovered by an organic refractory material formed by the accretion of light elements in molecular clouds and subsequent UV photoprocessing. In addition, two populations of smaller and homogeneous grains of graphite and silicates are needed to explain the whole spectral range of extinction data. One positive aspect of the above model is the evolutionary context in which the grain properties are defined. The size distribution of the large grains,

$$n(a) = exp\left\{-5\left(\frac{a - a_C}{a_i}\right)^3\right\} \tag{4}$$

is a modification of the Oort-Van de Hulst distribution, where a_C represent the core size, assumed fixed, and a_i, the decay rate of the distribution. Hence, all the big grains are assumed to have cores of same size, while the mantles have distinct thickness, according to the above size distribution. These grains are assumed elongated in such way that they are also responsible by the polarization. Hong & Greenberg (1980) have used a single size for the bare particles. Here, however, we have adopted for the bare grains the same size distribution for the core-mantle particles, but with a_C not related to a core size, but defining the initial size of the distribution. Again, silicon is a major constituent of two populations: the bigger coated grains and the small homogeneous grains of silicate. It is then necessary to determine the fraction of Si in these two populations. Contrary to the MRN model, we have two completely unrelated distributions and no boundary condition

can be obtained. We calculate the necessary Si abundance to reproduce the observed degree of polarization (whose size parameters have been previously fit using the polarization wavelength dependence); the fractions used in the extinction are then automatically fixed, assuming the total abundance known.

In general, the results of varying the extinction parameters are very similar to the MRN model. The consequences of the different shapes of the size distributions can be better illustrated in the polarization case when there is only one grain population. Changing a_c is very analogous to varying a^{sil}_- in the MRN model. However, while the maximum size of the MRN model only changes the size cutoff, a_i also modify the shape of size distribution (Fig. 6). A larger a_i makes the size distribution fall off more slowly, in such way that the larger grains have a greater weight. In addition, when the astronomical silicate is replaced by enstatite, the polarization curve is only slightly changed, since the mantle is thick enough to prevail on the optical behavior of the grain.

2.3. DWJ model

For the polarization fits, we have also considered the DWJ model (Duley et al. 1989). In this case, the polarization is produced by core-mantle grains with a power law size distribution following the assumptions of M86. The nucleus are compounded by silicates with a thin mantle of amorphous carbon. They considered that the mantle is thin enough to make the optical properties of whole grain be determined only by its nucleus; the compound suggested to represent this situation was basaltic glass (Lamy 1978; Pollack et al. 1973). The practical difference between this and the M86 model is then the index of refraction of the particles. Basaltic glass behaves similarly to enstatite as compared to astronomical silicate, and simulates small grains of that type.

3. DUST MODELS AND THE SMC DATA

We have supposed that the interstellar grains can be represented by the same size distribution adopted in the Galactic models, but probably with different parameters, in sense that the distribution width and average size are distinct. This situation might be achieved by the processes of grain formation and evolution in an environment of different metallicity. We have thus developed a computational code that searches for the best size parameters (within the scenario of a given model) fitting an observational (polarization or extinction) curve. For the models based on a power law size distribution, we have used an index of -3.5 (MRN), with the minimum and maximum sizes considered as free parameters. On the other hand, for the modified Van de Hulst-Oort size distribution of Greenberg and collaborators, we have assumed the core size, a_C, and the decay parameter, a_i, as free parameters. The parameters of the models are described in the section 2.

Our aim is to reproduce simultaneously the polarization as well as the extinction curve. Our approach was to perform initially the polarimetric fits; obtaining the sizes of anisotropic particles, they were carried over as fixed parameters in the fits of extinction.

To fit the wavelength dependence of the polarization, the Si abundance does not need to be specified. For the extinction, however, the relative abundances between carbon and silicon must be known. We have taken this ratio from the work of Dufton, Fitzsimmons & Horwarth (1991), which provides the abundances of C, Si and other elements in the atmosphere of a main sequence B-type star in the SMC. These numbers possibly represent

the present ISM abundance in that galaxy. This carbon abundance is consistent with a SMC metal abundance around 0.8-1.0 dex smaller than the Galactic one. Barbuy et al. (1991), in a study of cool supergiants, also found carbon abundances consistent with the other "heavy" elements. Besides, the N abundance indicates no contamination of processed material in the atmosphere, which suggests that this C abundance may represent the ISM. Dufour, Shields & Talbot (1982) and Dufour (1984) found a C abundance in the SMC HII regions around 1.5 dex smaller than the Galactic ones. If this value really represent the ISM, it might be consequence of a possible C depletion in grains. De Boer (1991) suggested a normal depletion (stellar "minus" interstellar) of the elements in the LMC relative to the Milky Way, however there was not data available to the SMC. So, it is possible that the depletion of the elements in the SMC ISM be similar to that in the Galaxy. We took the Si depletion equal to 1, i.e., all available silicon in the ISM is in the form of grains, analogously to what occurs in the Milky Way, where the Si depletion is practically total. On the other hand, the correct fraction of carbon in solid particles is not well determined in our Galaxy, but may range between 0.30 and 0.60 (Gondhalekar 1985a; Jenkins 1987); a dependence with the environment density is not discarded (Gondhalekar 1985a,b). We have thus performed fits using different values of C depletion, namely, 0.10, 0.25, 0.50, 0.75 and 0.90.

3.1. Data

The SMC optical polarimetric sample consists of the six stars: AZV126, AZV211, AZV215, AZV221, AZV398 and AZV456 (Magalhães et al. 1993). The object catalogue name are from Azzopardi & Vigneau (1982). The ISM characteristics of the above lines of sight are presented in the Table 1. This sample can be divided in two groups, according to

the colour behavior of the polarization. One is characterized by small λ_{max} compared to the Galaxy, but with normal widths, while the second has narrow curves (large values of K) with normal values of λ_{max} (Magalhães et al. 1993).

For the extinction fits, we have considered two kinds of UV extinction curves: the AZV398's (Prevot et al. 1984; Magalhães et al. 1993) and the AZV456's curve (Lequeux et al. 1984; Magalhães et al. 1993). The AZV398's extinction curve has no bump and an enhanced UV extinction, while the AZV456's has an extinction curve very similar to the Galaxy, but with its bump shifted to bluer wavelengths (Magalhães et al. 1993). Bouchet et al. (1985) found similar IR extinctions for a whole group of SMC stars which included these stars. We have hence taken the same IR extinction for the two extinction curves. These stars are also among the most reddened ones in the SMC.

3.2. Fits to the polarimetric data

This will not be the case however in the SMC fits, as very narrow size distribution will be used, and consequently very thin mantles. << encaixar em algum lugar

In this section, we summarize the parameters that result from the fits to the observed interstellar polarization in the SMC. The parameters related to the cylinder size distribution are $a^{sil}{}_p$ and $a^{sil}{}_+$ in the MRN and DWJ model and a_c and a_i in the Greenberg's model. The angle between the magnetic field and the plane of sky, γ, is taken as fixed and the fits are made using three values, 10^o, 30^o e 60^o. We used the MRN, M86 and Greenberg's models for all stars and for two stars, AZV398 and AZV456, also the

DWJ model and two kinds of silicates, namely, astronomical silicate and enstatite, have been used. The parameters corresponding to the results of the fits of all stars are listed in the Table 2, as well as the average sizes. The Figs. 8 to 10 illustrate the results, where we also show the extrapolation of the fits to the UV.

The star AZV126 has the smallest λ_{max} of the sample (0.31 $\pm$ 0.31 μm) with the maximum observed polarization in the U filter. This situation also happens to other stars in the sample and is one of the reasons for the large errors in the λ_{max}. The fits reproduce the data and the average sizes are the smallest among all the stars, consistent with the extreme λ_{max}. The sizes are spread over a narrower interval as compared to the Galactic distribution. The UV extrapolations for the MRN model (Fig. 8) show a large dispersion for the distinct γ's because of the poorly defined maximum. The larger values of γ produce smaller λ_{max}; the best fit is for $\gamma = 10^{o}$. The other models also reproduce the position of the λ_{max} obtained fitting the Serkowski law to the observations. To this star it would be interesting to have more measurements of polarization in other regions of the spectrum, precisely in the UV, to better define its maximum and also the width of its polarization curve.

The star AZV211 is special in respect to the width of its size distribution. It is the only star for which the fit of the Serkowski parameters provide a value of K **smaller** (broader polarization curve) than the obtained using the Galactic K x λ_{max} relation (Magalhães et al. 1993). While the size distribution produced by the MRN model has a width comparable to the Galactic one, the average size is smaller. The other models, however, follow the tendency of the other stars of having a narrow size distribution. The resulting polarization curves differs mainly in the UV extrapolation; for smaller γ, the MRN fits produce higher

polarization.

AZV221 follows the SMC trend. It has a small λ_{max} and a normal K. The resulting parameters confirm this tendency, it has a narrow size distribution with small average sizes. The fits are very good.

The star AZV398 has the highest polarization known in the SMC (Magalhães et al. 1993). The models are able to reproduce well the data (Fig. 9). The average sizes obtained are close to the Galactic values, but smaller. Its size distribution is quite narrow, confirming the tendency shown by the large value of K (Magalhães et al. 1993). For the MRN and Greenberg's model, it have been performed the fits replacing the astronomical silicate by enstatite. The fits do not show important differences, but the MRN models tends to have smaller values of χ^2 with enstatite (Table 2). The value of $\langle a \rangle$ obtained with enstatite is slightly greater than the obtained using the astronomical silicate (see section 2.1). Similar conclusions can be drawn for the DWJ model.

The star AZV456 possesses a very narrow polarization curve, with $K = 2.06 \pm 0.53$, quite extreme even for Galactic stars with large λ_{max} (Magalhães et al. 1993). In the sample of Whittet et al. (1992), the stars possessing the greater values of K (1.89, 1.81 and 1.59) have λ_{max} greater than 0.75 μm, which shows that the AZV456 is, to same extent, different from the Galactic stars. Also AZV215 has a large value of K for its λ_{max}. However, this star has polarimetric data in only four bands, which makes any conclusion necessarily uncertain. While the stars with small λ_{max} can be easily reproduced, i.e., there is always a size distribution able to fit the data, the stars AZV456 and AZV215 stars are not so easily fit. The best results are found for two situations: small values of γ or a

narrow size distribution. The MRN model illustrate the first case. The fit for $\gamma = 10^o$ presents an important improvement relative to the other angles, which have very broad curve. However, in any case the reddest point of the AZV456 (0.82 μm = 1.22 μm^{-1}) is not well fit (Fig. 10); values of γ smaller than 10^o do not improve the fit. In the second case, a narrow size distribution could not also completely reproduce the data. The polarization curve of a single size is characterized by ripples, the smoothness of the models only achieved by the use of a relative large size distribution. In order to fit the optical polarization of AZV456, the narrow size distribution produces a bump in the UV (Fig. 10). In the Greenberg's model fits, the bump is present for $\gamma = 60^o$ (near UV) and $\gamma = 30^o$ (begins at visible wavelengths). The DWJ model has or broader curves ($\gamma = 30^o$ and $\gamma = 10^o$) or a bump ($\gamma = 60^o$). The enstatite does not modify the results described above. Although there are no UV data, the presence of a bump is not probable. Hence, it seems that the reason of the narrowness of the polarization curve could be related with other properties of the grains. As claimed by Wilking et al. (1980), the increase of the real part of the index of refraction can produce narrow polarization curves. We have performed some fits using hypothetical compounds represented by a same index of refraction throughout the spectra. It is obviously a very crude hypothesis, but it may provide some insight in the consequences of changing the indexes of refraction. We have varied the real part of index of refraction from 1.7 to 2.0 and the imaginary part from 0.01 to 0.05. The variation in the polarization curve is very small and changes in the index of refraction (which roughly represent the silicates) are not enough to improve the results. The average sizes are Galactic, confirming the claimed relation between λ_{max} and the average sizes. More data in other spectral regions would be rewarding.

For some specific models, more than one set of parameters have been able to reproduce

the data. The sets represent two minimum of the χ^2. Obviously, one of them is only a local minimum. It can be interesting however to keep both size distributions in order to verify the influence of different anisotropic grain sizes when fitting the extinction. Examples are the fits of AZV211 (M86, $\gamma = 60^o$, astronomical silicate) and AZV398 (MRN, $\gamma = 60^o$, enstatite) (Table 2). The average sizes that define the size distributions are approximately the same, the main difference residing in their widths.

It may be noted that the average grain size decreases as γ increases (Table 2), which can be understood if one considers the geometric space defined by the rotation of a grain. Under a magnetic field with a large component in the line of sight (i.e., greater γ), the geometric space described by the rotating grain is greater (and more isotropic) than the one produced for a smaller γ. Under that condition, the grain looks larger and, in order to produce the same polarization, one needs a smaller size than with a small γ. Average sizes obtained for different models at a given γ are basically the same. The polarizing efficiency is greater to smaller γ, due to the greater anisotropy.

In short, the best results are achieved for stars having smaller λ_{max}. These stars have their polarization curve fit for any choice of γ or adopted model and the average sizes are smaller than the Galactic ones. The second group, formed by the stars AZV456 and AZV215, has very narrow curves, not easily reproduced by the above models. For these stars, small values of γ and narrow size distributions tend to produce best fits, but even in these cases a complete agreement with observations is not achieved. Changes in the index of refraction did not seem to be able to improve the results. For most stars, data in other spectral regions and with more spectral resolution would help to constrain the shape of the curve and hence the properties of the polarizing grains.

3.3. Fits to the extinction curves

We have performed fits to the extinction of two stars: AZV398 and AZV456, which should be representative of the two kinds of extinction curve found in the SMC. AZV398 possesses a typical SMC extinction curve, while AZV456 have an extinction similar to the Galactic one. These stars are also among the more reddened ones in the SMC and have relatively high polarization.

Our approach was to perform initially the polarimetric fits (see section 3.2) and, with the sizes of the anisotropic particles thus obtained, perform the extinction fits. The number of free parameters depends on the specific model. In the original MRN model, there are two populations of spherical grains: graphite and silicate. In this case, the numbers of parameter to be adjusted is four, since each size distribution needs two parameters to be specified: the maximum and minimum size. If the polarization is also considered, cylindrical silicate grains must be included. Their sizes are fixed by the polarization fits and the assumption of size distribution continuity also fixes the maximum size of the spherical silicate grains. We then end up with only three free parameters for the extinction fits, namely, the maximum and minimum graphite sizes and the minimum silicate size, a^{gra}_{-}, a^{gra}_{+} and a^{sil}_{-}, respectively. Concerning the Greenberg's model, the anisotropic particles are always present. Hence, with the sizes of the anisotropic particles fixed by the polarization, there are four free parameters related to the size distributions of spherical particles (graphite and silicates). We have always considered two kinds of silicates: the astronomical silicate and enstatite. Since their differences are important when fitting the

UV extinction.

3.3.1. AZV398

Table 3 shows the parameter fits of AZV398. It was excluded from this table the fits which had an excessive large χ^2. For this star, it is possible to find good fits using spherical grains of silicate and graphite, if less than 10% of the carbon is locked up in the grains (Fig. 11). This result is similar to that of Bromage & Nandy (1983) and Pei (1992). This is a direct consequence of the lack of the 2175 Å bump. The indexes of refraction of enstatite allow better results in the extremes of the extinction curve, compared to the astronomical silicate. The latter has an inflexion around 6.5 μm^{-1} after which the calculated extinction has a slope rather smaller than the observed. The fit in the IR is also poor with astronomical silicate. The average sizes are smaller than those for the Galactic extinction (Table 3), with the enstatite grains being smaller than the particles of astronomical silicate, although spreading over a larger interval. The graphite sizes are similar to the Milky Way ones, but these parameters are not important, since they can be modified without change in the general result, because the small contribution of graphite to the total extinction.

By including a population of anisotropic silicates particles fixed by the polarization fits, we have again obtained the best results in the case of small C depletions and for enstatite grains. Using the *size* continuity, only one set of parameters was able to reproduce that curve: the narrower size distribution of the cylindrical enstatite grains with $\gamma = 30^o$ and 10% of carbon in grains (Fig. 12). In this case, the whole extinction curve is well fit. The graphite grains have a small contribution, being marginally important in the IR. The main

IR and visible extinction fraction is produced by the cylindrical grains. For most fits, however, the *size* continuity is not able to reach a FUV extinction so high as the observed. For instance, for the astronomical silicate, we could not find a set of parameters able to reproduce even partially the extinction of AZV398. Considering the *volume* continuity, the relative contribution of spherical particles is increased making the FUV extinction higher. Hence, an easier agreement with the observation can be found. The best fit has been found for the broader size distribution of enstatite grains with a value of $\gamma = 30^{o}$ and 25% of carbon in the grains (Fig. 12). In this case, graphite has a contribution comparable to the cylinders in the IR and visible, and also its FUV extinction relatively important. Analogously to the "spherical" case, the astronomical silicate provides a poor agreement with the observations in the extremes. The best results correspond to $\gamma = 30^{o}$ and a C depletion of 10% (Fig. 12). Generally, the minimum size of the astronomial silicate tends to be smaller than the Galactic one. Nevertheless, the graphite average sizes can be smaller (astronomical silicate) or larger (enstatite). The most parameter sets that are not presented in the Table 3 are characterized by high C depletions and very large values of graphite sizes. When the graphite contribution is high enough to the bump be too pronounced, the sizes becomes larger trying to make the bump more shallow.

The relative number of carbon stars to normal stars in the post main-sequence stage is greater in the SMC than in the Milky Way (Lequeux 1988 and references therein). Therefore, it is not obvious that the SMC has a small number of carbon grains; necessary to fit the AZV398 extinction in the paragraphs below. As no bump is seen in this "typical SMC" line of sight, one might consider the extinction by grains of carbon not in the form of graphite. It have been argued that amorphous carbon grains are a more plausible interstellar component than graphite (Bussoletti, Colangeli & Orofino 1988 and references

therein). Studies of interplanetary dust shows that graphite is present only in trace amounts (Nuth 1985). Amorphous carbon has also been detected around R CrB stars (Hecht et al. 1984). Graphite, however, has been suggested to form in ISM by annealing process caused by the interstellar radiation field (ISRF) (Hecht 1986; Sorrel 1990). Hence, the SMC would be a privileged site for graphite formation because the ISRF is greater in the SMC than in the Galaxy (Lequeux 1989). As we have seen, that does not seem to be the case. It may be noted that in the lines of sight to AZV398 and AZV456, there are HII regions which have been identified as possible supernova remnants (SNR) (Davies, Elliott & Meaburn 1976). Only AZV456 has an extended IR, which suggest a possible dust condensation with processing by shock waves. Seab & Shull (1983) have been proposed a possible enhancement of the UV bump in SNR, but produced by a preferencial destruction of bigger and silicate grains. The line of sight of AZV456 is also characterized by the larger $\langle a \rangle$, discarding this possibility. However, the shock waves can be the agent of the graphitization of the amorphous carbon grains.Within this scenario, we have investigate the consequences of the replacement of the population of graphite grains by one of amorphous carbon particles, still in the framework of the MRN model. The optical constants were those given by Duley (1984).

Considering only spherical grains, very good fits can be achieved with both kinds of silicates (Fig. 13), but now the fraction of carbon in grains is substantially increased. For any value of C depletion both silicate and carbon contributions are important to the extinction. Better fits are found with astronomical silicate and large values of C depletion (Table 3). When amorphous carbon extinction is more prominent, the FUV extinction is better adjusted, as it reproduces well the FUV curvature. The silicate sizes are smaller than the Galactic and the size distribution has a cutoff at relatively smaller sizes, although

the average sizes are dependent of the depletion used. Enstatite produces an extinction that is able to reproduce the AZV398's extinction practically alone. So, when using this compound, it is possible to have two different kinds of fits. In one of them, the size distribution of the carbon grains are extended to very large sizes, in sense that its contribution is very small, and the enstatite respond for the most extinction. On the other hand, when the amorphous carbon is small, its contribution is comparable to the enstatite. Fig. 13 illustrates this behavior for a C depletion of 0.75.

If anisotropic particles are included, both types of continuities produce similar results. The best are found with small values of γ and great C depletions. Enstatite produces better results than the astronomical silicate. The best fit with astronomical silicate is found with a C depletion of 75%, $\gamma = 10^{o}$ and the continuity in the volume (Fig. 14); again, the FUV portion is only partially fit because of the saturation around 6.5 μm^{-1}. Using enstatite, the best results are achieved for the *size* continuity, C depletions of 75% and 90% and $\gamma = 30^{o}$ (Fig. 14). It is important to note that the contribution of the amorphous carbon in the IR is large. The grains of amorphous carbon have a size distribution considerably narrower than the Galactic size distribution of graphite. It can also be noted that the higher the contribution of the C grains, the greater the a^{sil}_{-}.

Greenberg's model does not produce good fits. When using astronomical silicates as the core compound of the polarizing particles, the saturation in the region of 6.5 μm^{-1} is very clear, although the IR and visible extinction are well fit. One example is found for the a C depletion of 90% and $\gamma = 60^{o}$ (Fig. 15). Note that this set of parameters have not the smallest χ^2, but its IR extinction is the best one. When using enstatite nucleus, reasonable fits are found for a C depletion of 50%, but the resulting value of R is quite small, less

than 2 (Fig. 15). The contribution of the cylindrical grains is small along the whole spectrum. Graphite is the major contributor to the IR and visible, being important also in the FUV. It is difficult to make a comparison with Galactic sizes since it have been used a different size distribution for the bare particles.

In conclusion, the MRN model is able to match the data. The models using enstatite produce sligthly better results, mainly because the FUV region. The silicates grains, in average, are smaller than in the Galaxy. The MRN model with anisotropic particles of astronomical silicate and *size* continuity is not able to reproduce the data. In this case, the *volume* continuity must be used. When using graphite, the AZV398 extinction can only be fit if we have a small number of carbon grains. However, amorphous carbon allows also a very good match with observations with a relatively large fraction of C in form of grains. Concerning Greenberg's model, we were not able to find a set of parameters able to reproduce the whole extinction curve.

3.3.2. AZV456

AZV456 shows the 2175 Å extinction bump. A graphite population, or another compound able to reproduce the UV bump, should be then included. The best results are presented in the Table 4.

Models using spheres of silicates and graphite are able to reproduce well the data (Fig. 16). Both types of silicate allow similar results, but again the FUV extinction of enstatite allows a slightly better agreement. Both kinds of silicate produce the best results for 25% of carbon in grains, but using 50% the fits are also very good (Table 4). When more

carbon is used, their sizes have to be increased in order to have the same bump strength, as an increase in size results in shallow bump. Also the IR contribution of carbon grains becomes greater. So the average sizes of graphite and silicate decrease for larger C depletions. The models with enstatite provide graphite sizes larger than those with astronomical silicate. This is because enstatite has an increase in extinction around 4.4 μm^{-1}, near the bump, so the graphite contribution has to be smaller, which implies larger sizes. Is both cases, however, the sizes tend to be smaller than the Galactics. It should be emphasized that the bump is not well reproduced, as its extinction peak is always above the model curve. The calculated bump position is also always redder than the observed.

The MRN model with silicate divided in spheres and cylinders is able to reproduce the AZV456's extinction. In general, the fits using the *volume* continuity are better than using the *size* continuity and enstatite produced definitely better results. When using the *size* continuity, reasonable fits can only be achieved for the small values of γ. The best fit using astronomical silicate is found for the *volume* continuity, a C depletion of 90% and a γ of 30^o (Fig. 17). The two best fits using enstatite are also found for the *volume* continuity (Fig. 17). The graphite contribution is important in the visible and IR. Their average sizes are grater than the Galactic, but with a narrow size distribution. The a^{sil}_{-} is similar to the Galactic one. All fits produce a bump shifted to redder wavelengths.

Most fits using the Greenberg's model have quite a small contribution from graphite, making it difficult to reproduce the observed extinction curve. There is, however, one set of parameters able to reproduce the AZV456's data. It uses enstatite, a C depletion of 25%, and the $\gamma = 10^o$. The bump is redder and the FUV extinction somewhat more enhanced than the observed (Fig. 18)

In short, all the fits present the bump redder than the observed. We have, then, tried to change the parameters of the graphite distribution in both models, but no improvement could be achieved. It would be interesting to perform the calculation using another form of graphite grains. It was argued that small prolate spheroids can shift the bump position to bluer wavelengths (Draine 1988). It must be remembered that graphite particles in spherical shapes are not probable, since the graphite tend to be formed in anisotropic shapes (Czyzak, Hirth & Tabak 1982). Analogously to AZV398, Greenberg's model is not able to reproduce the data.

3.4. Necessary abundances to fit the observed polarization

In section 3.2 above, we have fit only the spectral dependence of the polarization. We can also obtain the necessary abundance of Si/H from observed percentage of polarization. The observed Si abundance in the SMC is 6.88 dex (Dufton et al. 1991). The necessary abundances decrease with γ, as the polarizing efficiency of the grains increases with smaller γ (section 3.2). Among the models, the one from Greenberg and collaborators needs the smaller quantity of Si, because the polarizing grains are not formed entirely by silicate, having a mantle made of lighter elements. Basically, all stars need a quantity of Si available in the SMC interstellar medium, the exception being AZV456, which needs more. This star has a Galactic gas-to-dust ratio; its color excess is similar to that of AZV398, so the small ratio is interpreted as a small quantity of gas, and it needs more silicon to hydrogen than the other stars. The gas-to-dust ratio was obtained taking in account only the HI (Bouchet et al. 1985); if this line of sight has a considerable quantity of H_2, less Si will be needed. Schwering & Israel (1990) have detected a extended IR

source coincident with AZV456 which may possibly be associated with H_2 population.

3.5. A(V) and P(V)/A(V)

From the extinction and polarization fits the total extinction in the visible, A(V), and the ratio between the polarization and extinction, P(V)/A(V) may be obtained. A(V) is a measure of the total amount of dust and its extinction efficiency in a given line of sight. It can be obtained observationally through the values of R and E(B-V) (Table 1). For the AZV398, considering the larger uncertainties involved, we have found (Table 3) a good agreement with the observed value (within a factor of 2) with a tendency for the best models provide greater values of A(V). On the other hand, the values found for AZV456 (Table 4) are smaller than the observed (a factor of 5). Analogously to the abundance, a larger gas-to-dust ratio would improve the results (see section 3.4 above). On the average, astronomical silicate and amorphous carbon produce more extinction compared to enstatite and graphite, respectively.

The P(V)/A(V) ratio is not dependent of the abundance, but it is a characteristic of a given model. The observed ratios are presented in the Table 1. For AZV398, the calculated ratio is very high, except in Greenberg's model. However, such models are not able to reproduce the extinction curve. Concerning the MRN model, this high P(V)/A(V) means that the contribution to the extinction of the polarizing grains is too high. We found practically the same results for AZV456. In this case, Greenberg's model, however, do not produce smaller ratios, being the best fit a good example of this behavior.

4. CONCLUSIONS

The main conclusions of this work can be summarized as follows:

1. The SMC polarization curves possessing small λ_{max} and normal K values may be better fit with popular grain models than those possessing normal λ_{max} and narrow polarization curve. For the latter, small values of γ, the angle between the magnetic field and the plane of the sky, and narrow size distributions tend to produce best fits, even though a satisfying agreement with observations is not achieved. Extension of the spectral range covered by the polarization data in the SMC would be highly desireable.

2. The 'typical' SMC extinction curve can be fit using the MRN silicate-graphite model and a small carbon depletion. If carbon is in amorphous form, good results are still obtained without the assumption of a small amount of carbon in grains.

3. The extinction curve (similar to our Galaxy) of AZV456 can be fit by the MRN model, but the bump position is not well reproduced. The calculated bump is at redder wavelengths than the observed one. This might be a consequence of anisotropic shapes of graphite particles.

4. The mantle-coated silicate model does not succeded in fitting the extinction curves in the SMC.

5. In general, the SMC data (polarization and extinction) are fit using distributions which

are narrower and shifted to smaller wavelengths relative to the Galaxy.

6. A dust model that fits the extinction may have difficulties fitting both extinction and polarization consistently. This is because the inclusion of cylindrical (say) particles that fit the polarization may significantly affect the extinction as well.

7. We have studied two different ways of fixing the ratio between the number of spherical and cylindrical silicates, namely size continuity and volume continuity. Fits using volume continuity, which implies a larger number of spheres, resulted in better fits. A physical justification for such distribution should be still further studied however.

8. A possible scenario for the SMC is that, in the more diffuse regions, the carbon grains are in amorphous form, despite the more intense radiation field. The data for AZV 456 suggest however that, in the regions that have been sujected to shock waves, these grains might have been graphitized.

ACKNOWLEDGEMENTS

This work has been supported by NASA Grant NAG 5 1463. It has been also partially supported (C.V.R.) by FAPESP (Proc. 89/3091-6). The programs have been run in the VAX8530/VMS and the SPARCstations of the Department of Astronomy, Instituto Astronômico e Geofísico, Universidade de São Paulo. AMM and CVR would like to acknowledge the hospitality provided by Dr. A. Code, Space Astronomy Lab and Astronomy Department, Univ. of Wisconsin, where this research was partly done.

5. REFERENCES

Anders, E. & Grevesse, N. 1989, Geochimica et Cosmochimica Acta **53**, 197

Azzopardi, M. & Vigneau, J. 1982, A&AS **50**, 291

Barbuy, B., Spite, M., Spite, F. & Milone, A. 1991, A&A **247**, 15

Bohren, C. E. & Huffman, D. R. 1983, *Absorption and Scattering by Small Particles* (New York: John Wiley & Sons)

Bouchet, P., Lequeux, J., Maurice, E., Prevot, J. & Prevot-Burnichon, M. L. 1985, A&A **149**, 330

Bromage, G. E. & Nandy, K. 1983, MNRAS **204**, 29p

Bussoletti, E., Colangeli, L. & Orofino 1988, in *Experiments Cosmic Dust Analogues*, ed. E. Bussoletti, C. Fusco & G. Longo (Netherlands: Kluwer Ac. Publ.), 63

Chlewicki, G. & Greenberg, J. M. 1990, ApJ **365**, 230

Czyzak, S. J., Hirth, J. P. & Tabak, R. G. 1982, Vistas in Astr. **25**, 337

Davies, R. D., Elliott, K. H. & Meaburn, J. 1976, Mem. R. Astr. Soc. **81**, 89

Davis, Jr., L. & Greenstein, J. L. 1951, ApJ **114**, 206

de Boer, K. S. 1991, in *IAU Symp. 148, The Magellanic Clouds*, ed. R. Hayned & D. Milne (Netherlands: Kluwer Ac. Publ.), 401

Draine, B. T. 1988, ApJ **333**, 848

Draine, B. T. 1989, in *IAU Symp. 135, Interstellar Dust*, ed. L. J. Allamandola & A. G. G. M. Tielens (Netherlands: Kluwer Ac. Publ.), 313

Draine, B. T. & Lee, H. M. 1984, ApJ **285**, 89

Dufour, R. J. 1984, in *IAU Symp. 108, Structure and Evolution of the Magellanic Clouds*, ed. S. van den Bergh & K. S. de Boer (Netherlands: Dordrech-Reidel), 353

Dufour, R. J., Shields, G. A. & Talbot, R. J. 1982, ApJ **252**, 461

Dufton, P. L., Fitzsimmons, A. & Horwath, I. D. 1990, ApJ **362**, L59

Draine, B. T. & Lee, H. M. 1984, ApJ **285**, 89

Duley, W. W. 1984, ApJ **287**, 694

Duley, W. W. 1987, MNRAS **229**, 203

Duley, W. W., Jones, A. P. & Williams, D. A. 1989, MNRAS **236**, 709

Gondhalekar, P. M. 1985a, ApJ **293**, 230

Gondhalekar, P. M. 1985b, MNRAS **216**, 57p

Greenberg, J. M. 1968, in *Stars and Stellar Systems, Vol. 7, Nebulae and Interstellar Matter*, ed. B. M. Middlehurst & L. H. Aller (Chicago: Univ. Chicago Press), 221

Hecht, J. 1986, ApJ **305**, 817

Hecht, J. Holm, A. V., Donn, B. & Wu, C. C. 1984, ApJ **280**, 228

Hildebrand, R. H. 1988, Q. Jl. R. Ast. Soc. **29**, 327

Hong, S. S. & Greenberg, J. M. 1980, A&A **88**, 194

Huffman, D. R. & Stapp, J. L. 1971, Nature Phys. Sci. **229**, 45

Jenkins, E. B.1987, in *Astroph. Space Sci. Libr., Vol. 134, Interstellar Processes*, ed. D. J. Hollenbach & H. A. Thronson Jr. (Netherlands: Dordrech-Reidel)

Jones, R. V. & Spitzer Jr., L. 1967, ApJ **147**, 943

Lamy, P. L. 1978 Icarus **34**, 68

Lequeux, J. 1988, in *Dust in the Universe*, ed. E. M. Bailey & D. A. Williams (Cambridge: Cambridge Univ. Press), 449

Lequeux, J. 1989, in *Recent Developments of Magellanic Research*, ed. K. S. de Boer, F. Spite & G. Stasinska (Paris: Obs. Paris), 119

Lequeux, J., Maurice, E., Prevot, L., Prevot-Burnichon, M. L. & Rocca-Volmerange B. 1984, A&A **113**, L5

Lind, A. C. & Greenberg, J. M. 1966, J. Appl. Phys. **37**, 3195

Magalhães, A. M., Rodrigues, C. V., Coyne, G. V. & Piirola, V. 1993, in preparation

Martin, N., Maurice, E. & Lequeux, J. 1989, A&A **215**, 219

Mathis, J. 1979, ApJ **232**, 747

Mathis, J. 1986, ApJ **308**, 281 (M86)

Mathis, J., Rumpl, W. & Nordsieck, K. H. 1977, ApJ **217**, 425 (MRN)

Nuth, J. A. 1985, Nature **318**, 166

Pei, Y. C. 1992, ApJ **395**, 130

Pollack, J. B., Toon, O. B. & Khare, B. N. 1973, Icarus **19**, 372

Prevot, M. L., Lequeux, J., Maurice, E., Prevot, L. & Rocca-Volmerange, B. 1984, A&A **132**, 389

Purcell, E. M. 1979, ApJ **231**, 404

Roche, P. F., Aitken, D. K. & Smith, C. H. 1987, MNRAS **228**, 269

Sauvage, M., Thuan, T. X. & Vigroux, L. 1990, A&A **237**, 296

Savage, B. D. & Mathis, J. 1979, ARAA **17**, 73

Schwering, P. B. W. 1988, Ph.D. Thesis, University of Leiden

Schwering, P. B. W. & Israel, F. P. 1990, A&AS **79**, 79

Seab, C. G. & Shull, J. M. 1983, ApJ **275**, 652

Shah, G. A.1970, MNRAS **148**, 93

Sorrell, W. H. 1990, ApJ **243**, 570

Wheeler, J. C., Sneden, C. & Truran Jr., J. W. 1989, ARA&A **27**, 279

Whittet, D., Martin, P., Hough, J., Rouse, M., Bailey, J. & Axon, D. 1992, ApJ **386**, 562

Wilking, B. A., Lebofsky, M. J., Martin, P. G., Rieke, G. H. & Kemp, J. C. 1980, ApJ **235**, 905

Wolff, M. J., Clayton, G.C. & Meade, M.R. 1993, ApJ **403**, 722

FIGURE CAPTIONS

Fig. 1 : Extinction curves calculated using only spherical grains (**solid line**) and graphite spherical grains and silicate spherical and cylindrical grains (**dashed line**). The mean Galactic extinction curve is also shown (**dots**).

Fig. 2 : Extinction curves using the size continuity (**solid line**) and volume continuity (**dashed line**). The mean Galactic extinction curve is also shown (**dots**).

Fig. 3 : Extinction curves resulting from different values of a^{sil}_{p} (size of the largest silicate spherical grain which is the same as that of the smallest silicate cylindrical grain). The curves correspond to the values: 0.02μm (**solid line**); 0.04μm (**dashed line**) and 0.06μm (**trace-dot-trace line**). The dots represent the mean Galactic extinction curve.

Fig. 4 : Extinction curves resulting from different values of a^{sil}_{+} (size of the largest silicate cylindrical grain). The curves correspond to the values: 0.15μm (**solid line**); 0.19μm (**dashed line**) and 0.23μm (**trace-dot-trace line**). The dots represent the mean Galactic extinction curve.

Fig. 5 : Extinction curves resulting from different values of a^{gr}_{-} (size of the smallest graphite grain) and a^{gr}_{+} (size of the largest graphite grain). The curves for different values of a^{gr}_{-} are: 0.001μm (**solid line**); 0.005μm (**dashed line**) and 0.010μm (**trace-dot-trace line**). The curves for different values of a^{gr}_{+} are: 0.05μm (**solid line**); 0.01μm (**dotted line**) and 0.15μm (**trace-dot-dot-dot-trace line**). The dots represent the mean Galactic extinction curve.

Fig. 6 : Polarization curves obtained for different models and grain sizes. All curves are for a value of $\gamma = 10^{o}$. **Solid line**: MRN model with sizes between 0.055 and 0.25μm; **dashed line**: MRN model with sizes between 0.063 and 0.25μm; **trace-dot-trace**: MRN model with sizes between 0.055 and 0.20μm; **dotted line**: Greenberg's model with $a_c = 0.038\mu m$ and $a_i = 0.10\mu m$; **trace-dot-dot-dot-trace**: Greenberg's model with $a_c = 0.038\mu m$ and $a_i = 0.16\mu m$. The bars represent a typical Galactic polarization curve.

Fig. 7 : Polarization curves using indices of refraction of astronomical silicate (**solid line**) and enstatite (**dashed line**). The bars represent a typical Galactic polarization curve.

Fig. 8 : Fits to the polarization data of AZV126 using the MRN model. Results for different values of γ are shown: $\gamma = 60^{o}$ (**solid line**); $\gamma = 30^{o}$ (**dashed line**); $\gamma = 10^{o}$ (**trace-dot-trace line**).

Fig. 9 : Fits to the polarization data of AZV398 using different models and silicates. All curves have $\gamma = 30^{o}$. **Solid line**: MRN model with astronomical silicate; **dashed line**: MRN model with enstatite; **trace-dot-trace**: Greenberg's model and astronomical silicate and **dashed line**: Greenberg's model and enstatite.

Fig. 10 : Fits to the polarization data of AZV456 using different models and values of γ. **Solid line**: MRN model with $\gamma = 10^{o}$; **dashed line**: MRN model with $\gamma = 60^{o}$; **trace-dot-trace line**: Greenberg's model with $\gamma = 60^{o}$; **dotted line**: Greenberg's model with $\gamma = 30^{o}$; **trace-dot-dot-dot-trace line**: Greenberg's model with $\gamma = 10^{o}$.

Fig. 11 : Fits to the extinction data of AZV398 using the MRN model with only spherical particles of graphite and silicate. The **solid line** represents the fit for

astronomical silicate and the **dashed line**, for enstatite. The amount of carbon locked up in the grains is 5% for both curves.

Fig. 12 : Fits to the extinction data of AZV398 using the MRN model with spherical graphite and silicate particles and cylindrical silicate particles of sizes adjusted by the polarization fits. The spherical silicate particles have not been constrained by the cylindrical particles distribution. **Solid line:** enstatite, $\gamma = 30^{o}$, 10% of carbon in grains and size continuity; **dashed line**: enstatite, $\gamma = 30^{o}$, 25% of carbon in grains and volume continuity; **trace-dot-trace line**: astronomical silicate, $\gamma = 10^{o}$, 10% of carbon in grains and volume continuity;

Fig. 13 : Fits to the extinction data of AZV398 using the MRN model with only spherical amorphous carbon and silicate particles. The **solid line** represents the fit for astronomical silicate and 90% of carbon in grains; **dashed line**: enstatite and 75% of carbon in grains and **trace-dot-trace line**: enstatite and 75% of carbon in grains.

Fig. 14 : Fits to the extinction data of AZV398 using the MRN model and spherical particles of amorphous carbon and spherical and cylindrical silicate grains. The **solid line** represents the fit for astronomical silicate, volume continuity and 75% of carbon in grains; **dashed line**, enstatite, size continuity and 75% of carbon in grains and **trace-dot-trace line**: enstatite, size continuity and 90% of carbon in grains.

Fig. 15 : Fits to the extinction data of AZV398 using the Greenberg's model. The **solid line** represents the best fit achieved for silicates in form of astronomical silicate and 90% of carbon in grains. The **dashed line** represents the best fit for enstatite with 50% of carbon in grains.

Fig. 16 : Fits to the extinction data of AZV456 using the MRN model with spherical particles. In both curves, we have used 25% of carbon in grains. The **solid line** is the best fit for astronomical silicate and the **dashed line** for enstatite.

Fig. 17 : Fits to the extinction data of AZV456 using the MRN model with spherical graphite and silicate particles and cylindrical silicate particles of sizes adjusted by the polarization fits. The spherical silicate particles have not been constrained by the cylindrical particles distribution. **Solid line**: enstatite, 50% of carbon in grains, volume continuity and $\gamma = 30^{o}$; **dashed line**: enstatite, 25% of carbon in grains, volume continuity and $\gamma = 10^{o}$; **trace-dot-trace line**: astronomical silicate, 90% of carbon in grains, volume continuity and $\gamma = 30^{o}$.

Fig. 18 : Best fit to the extinction data of AZV456 using the Greenberg's model. The curve was obtained using enstatite, 25% of carbon in grains and $\gamma = 10^{o}$.

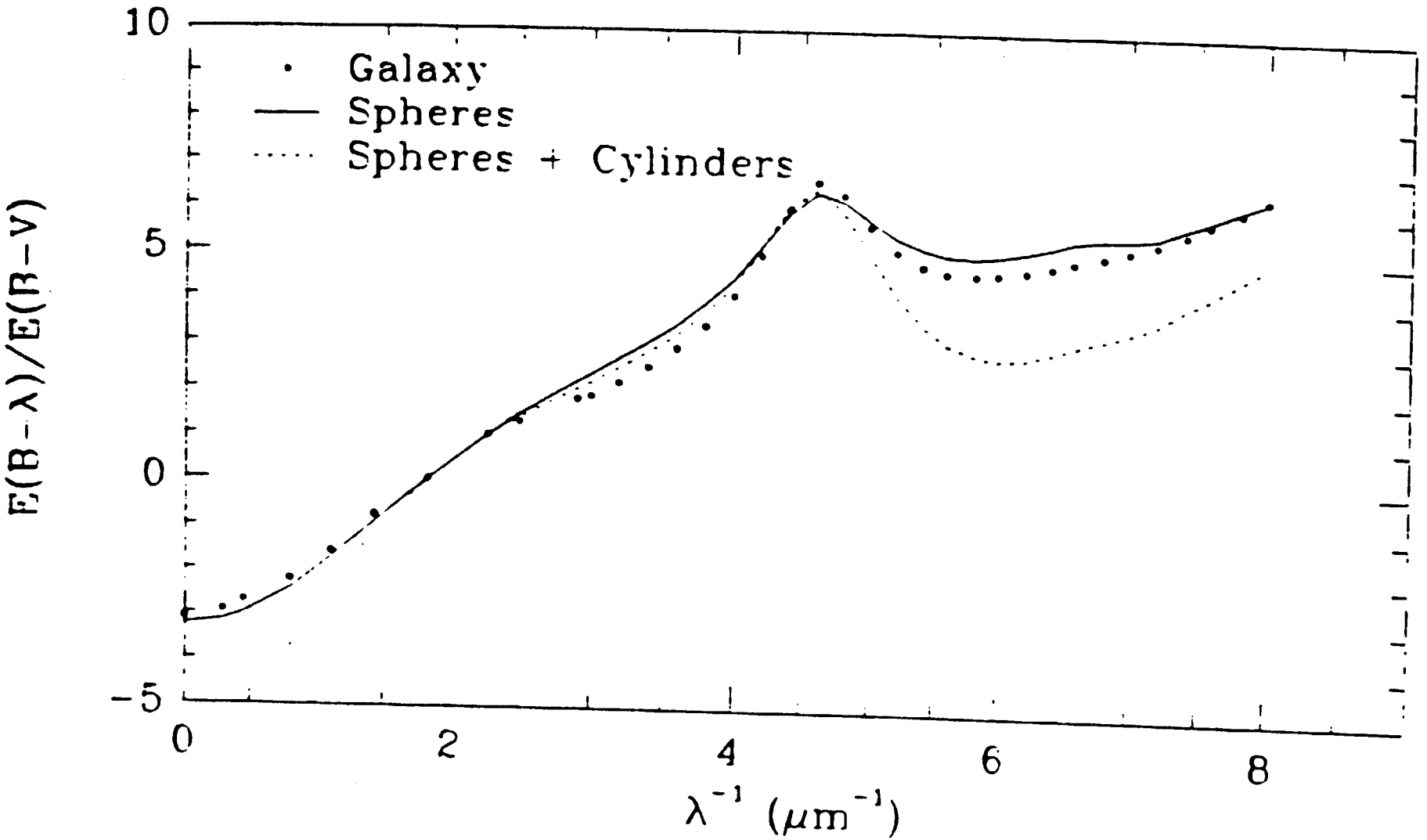
10
5
0
−5
0
2
4
6
8
Galaxy
Spheres
Spheres + Cylinders
E(B−λ)/E(B−V)
λ⁻¹ (μm⁻¹)

Fig 4

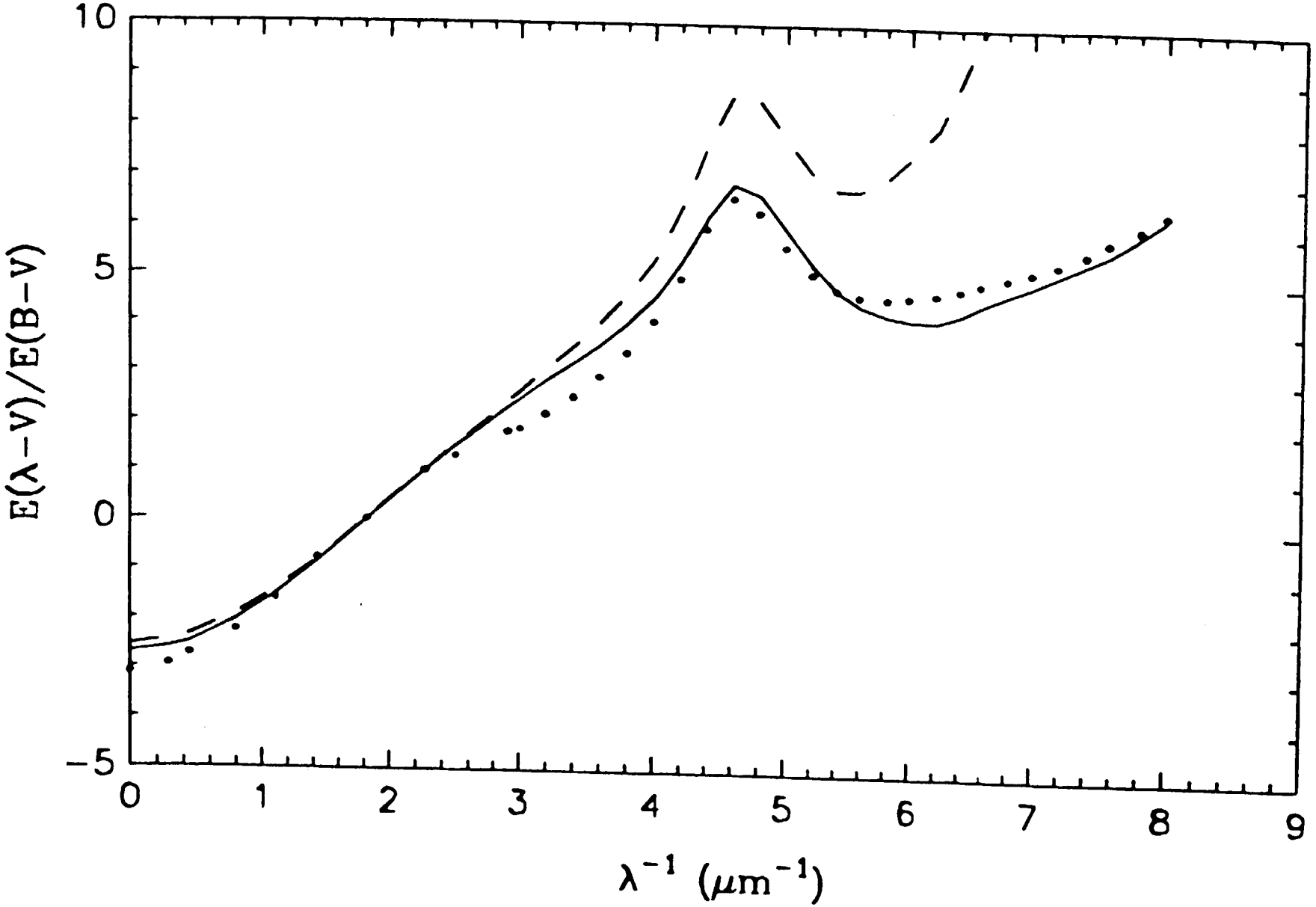

FIG. 2

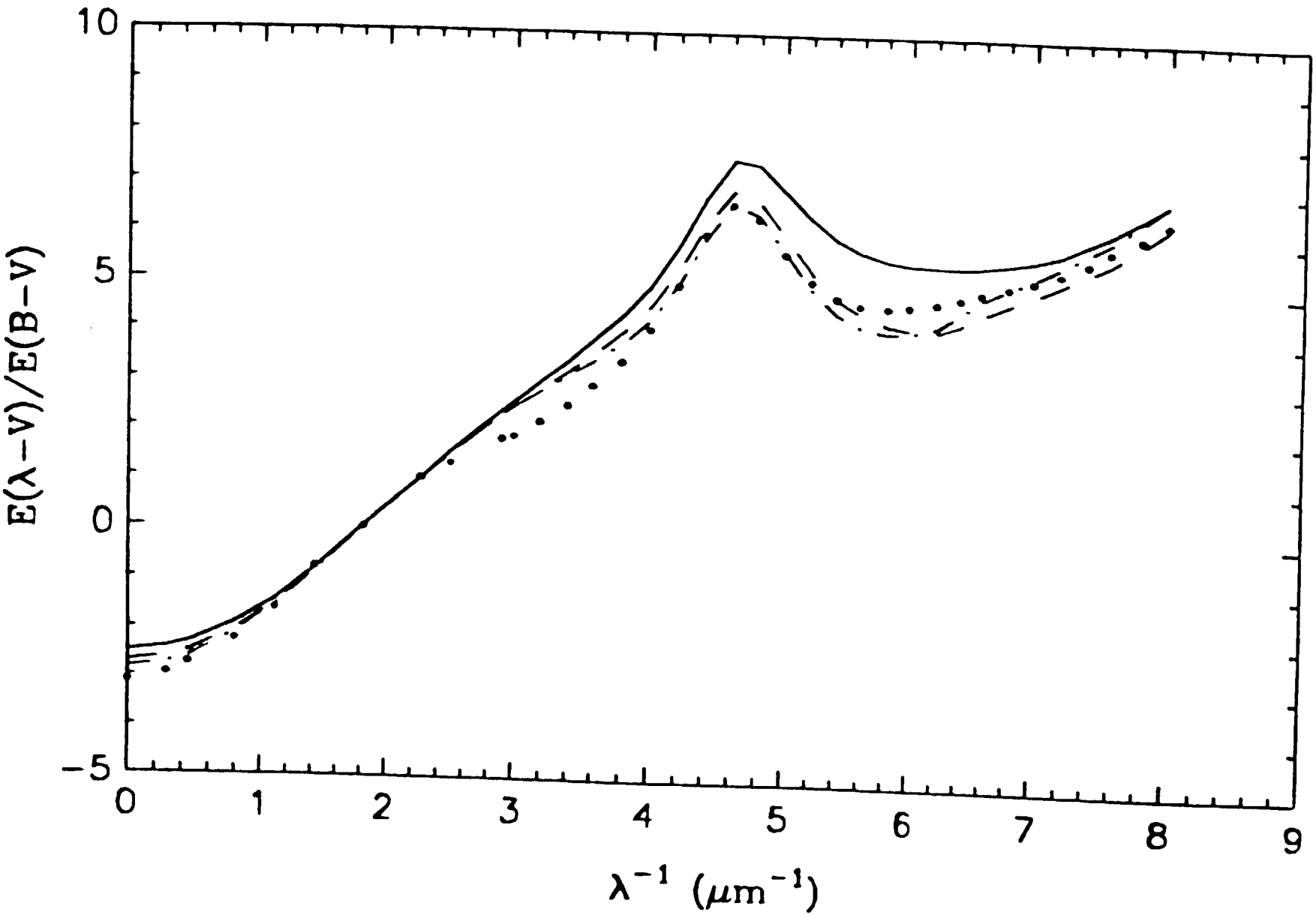

FIG 3

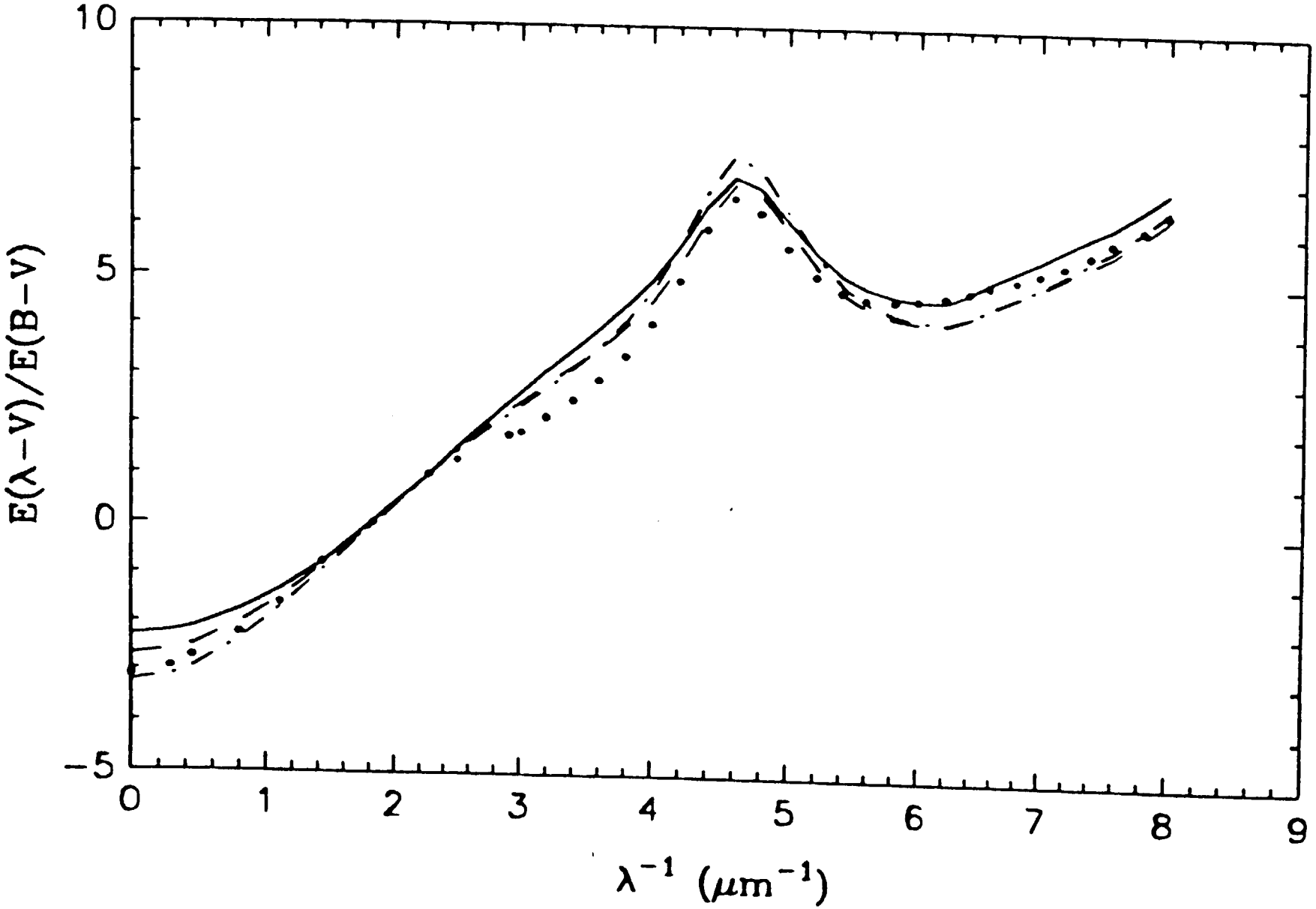
10
5
0
−5
0
1
2
3
4
5
6
7
8
9
E(λ−V)/E(B−V)
λ⁻¹ (μm⁻¹)

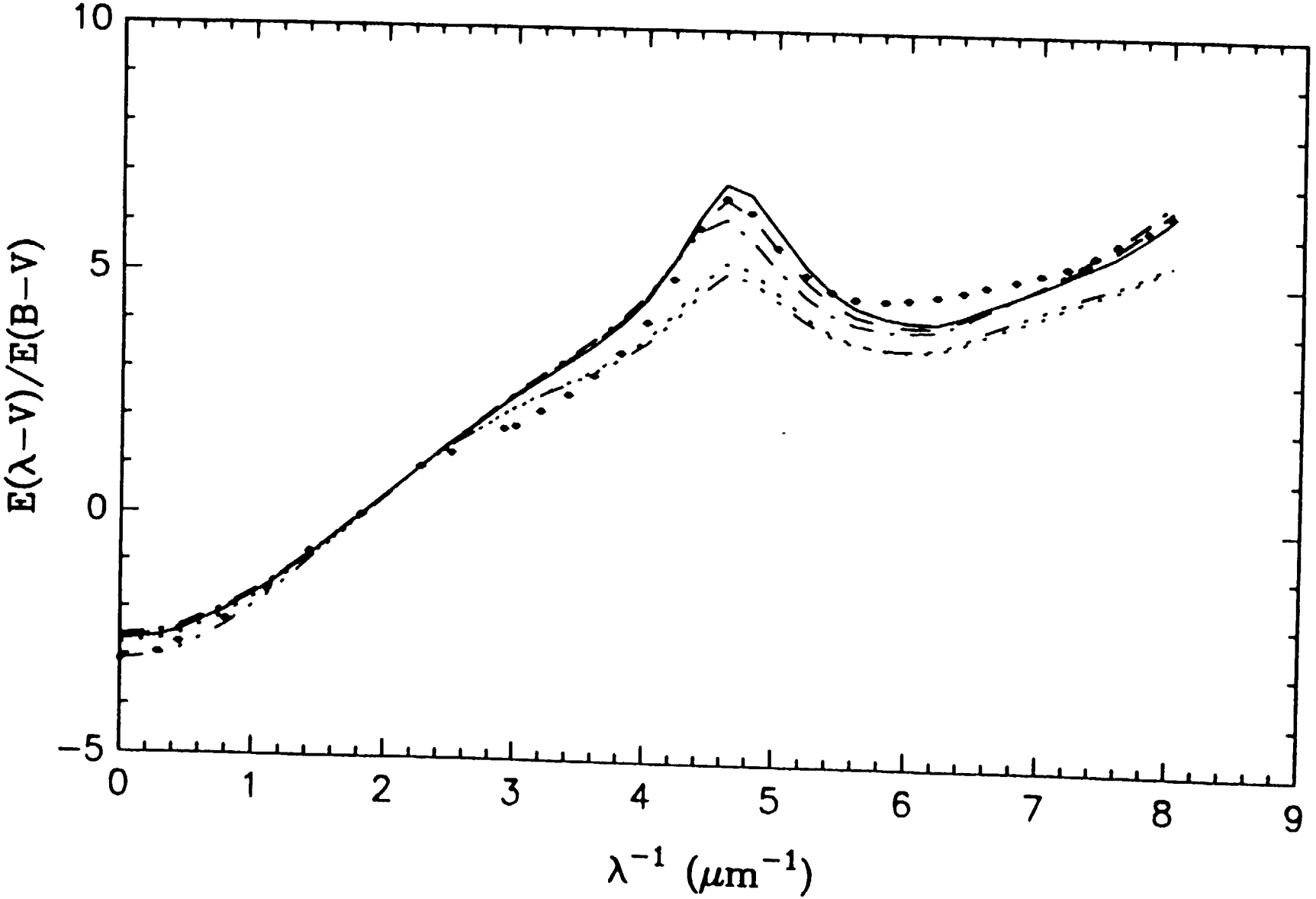

Fig 5

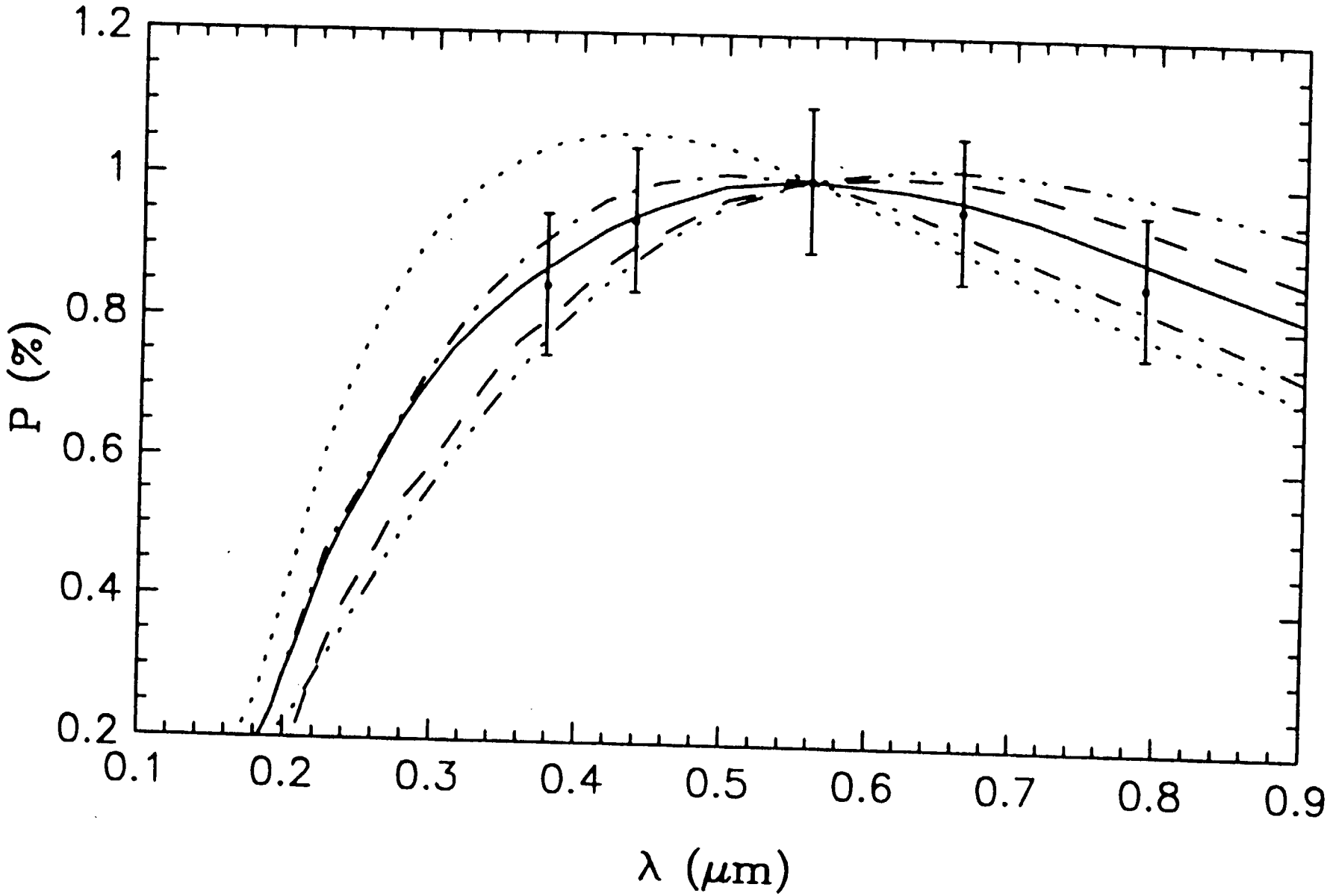

Fig 6

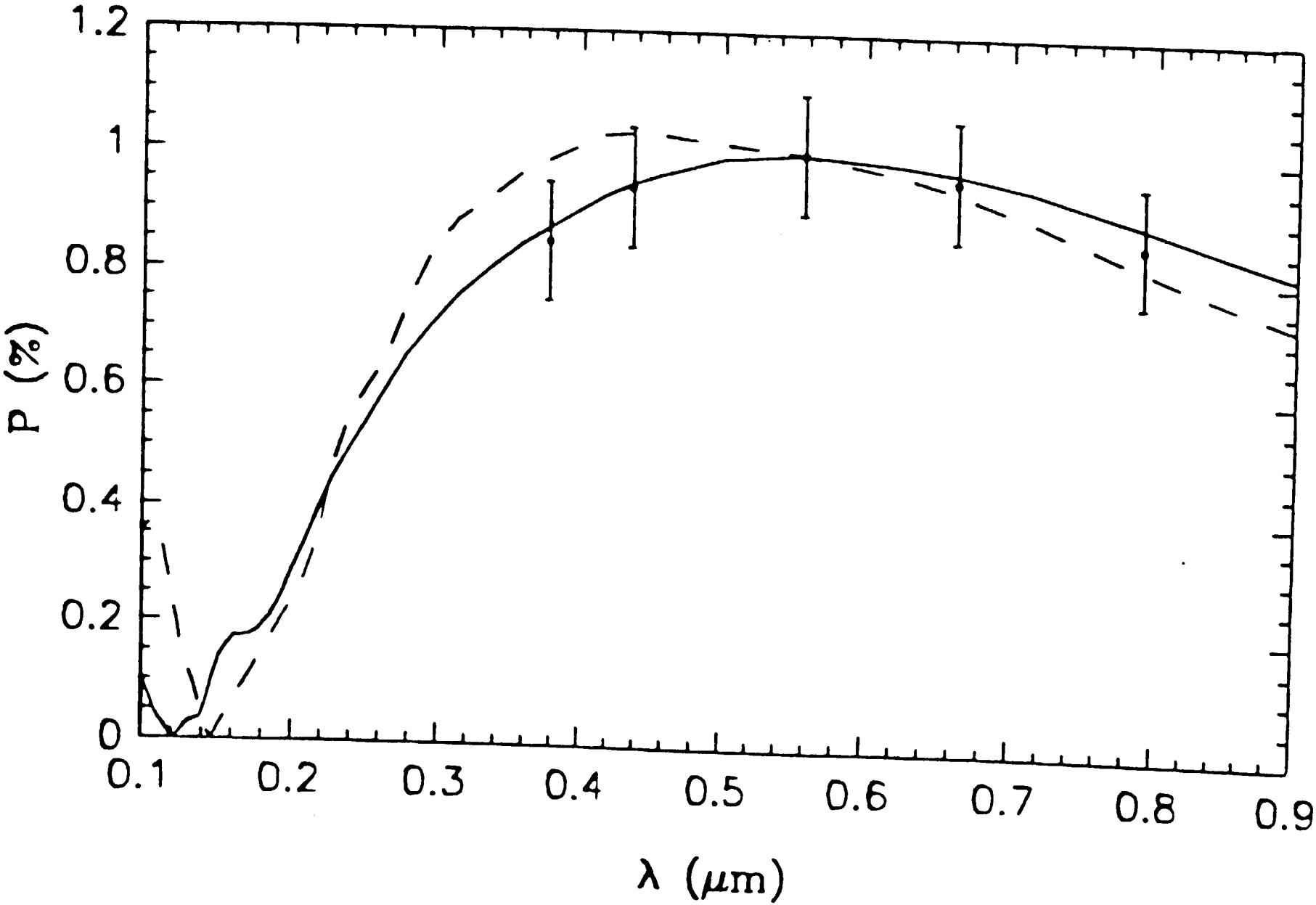

FIG 7

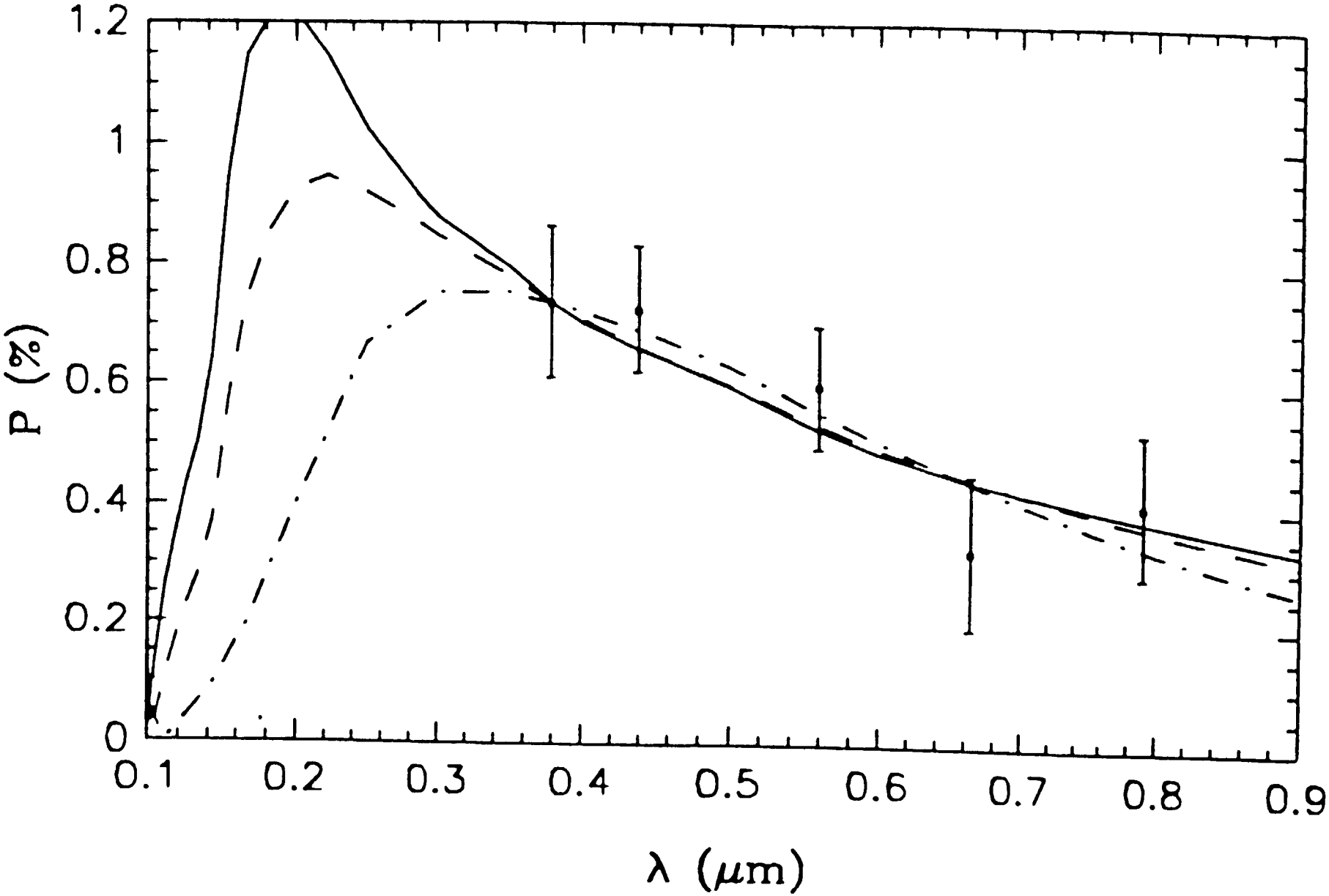
1.2
1
0.8
0.6
0.4
0.2
0
P (%)
0.1
0.2
0.3
0.4
0.5
0.6
0.7
0.8
0.9
λ (μm)

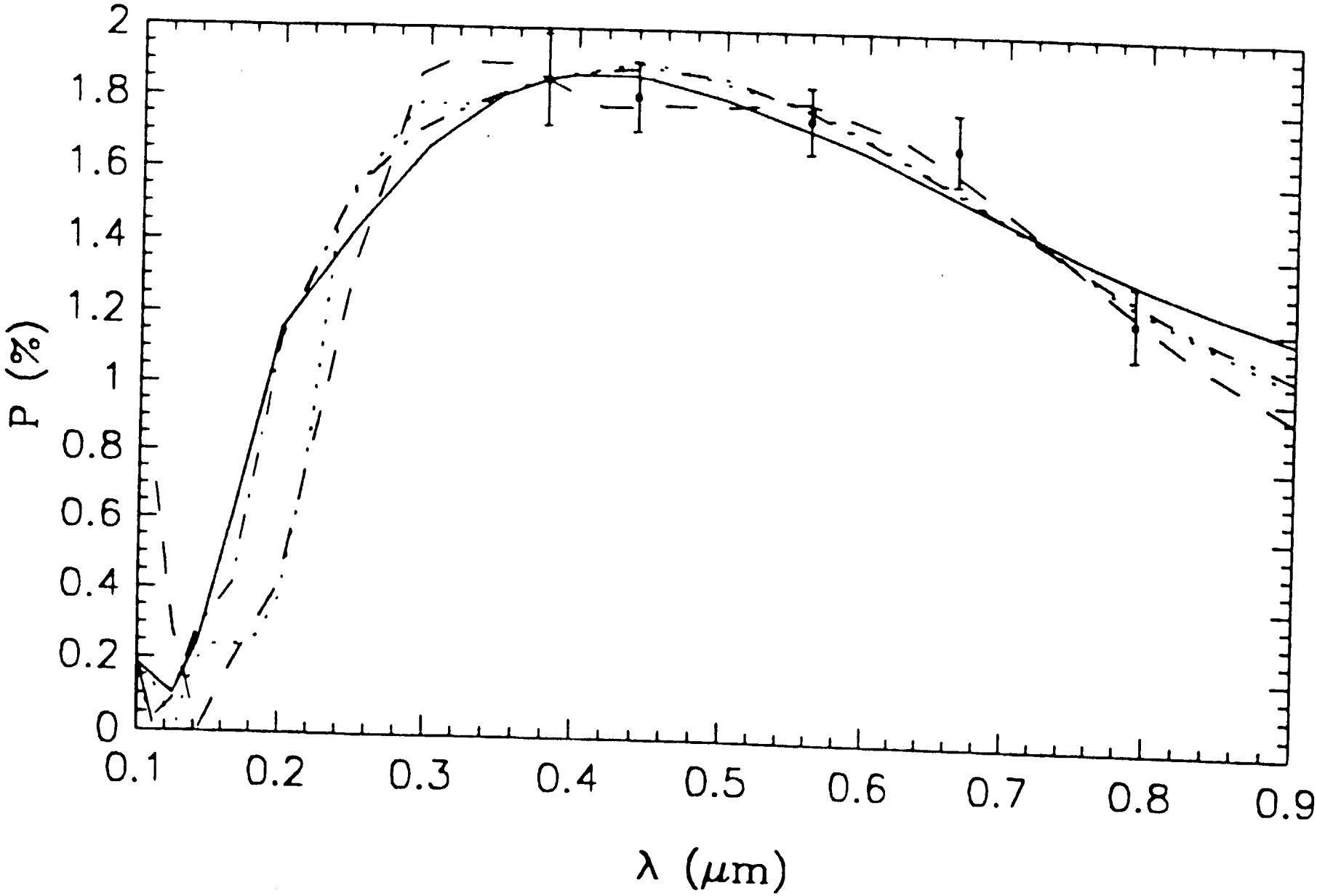

Fig. 9

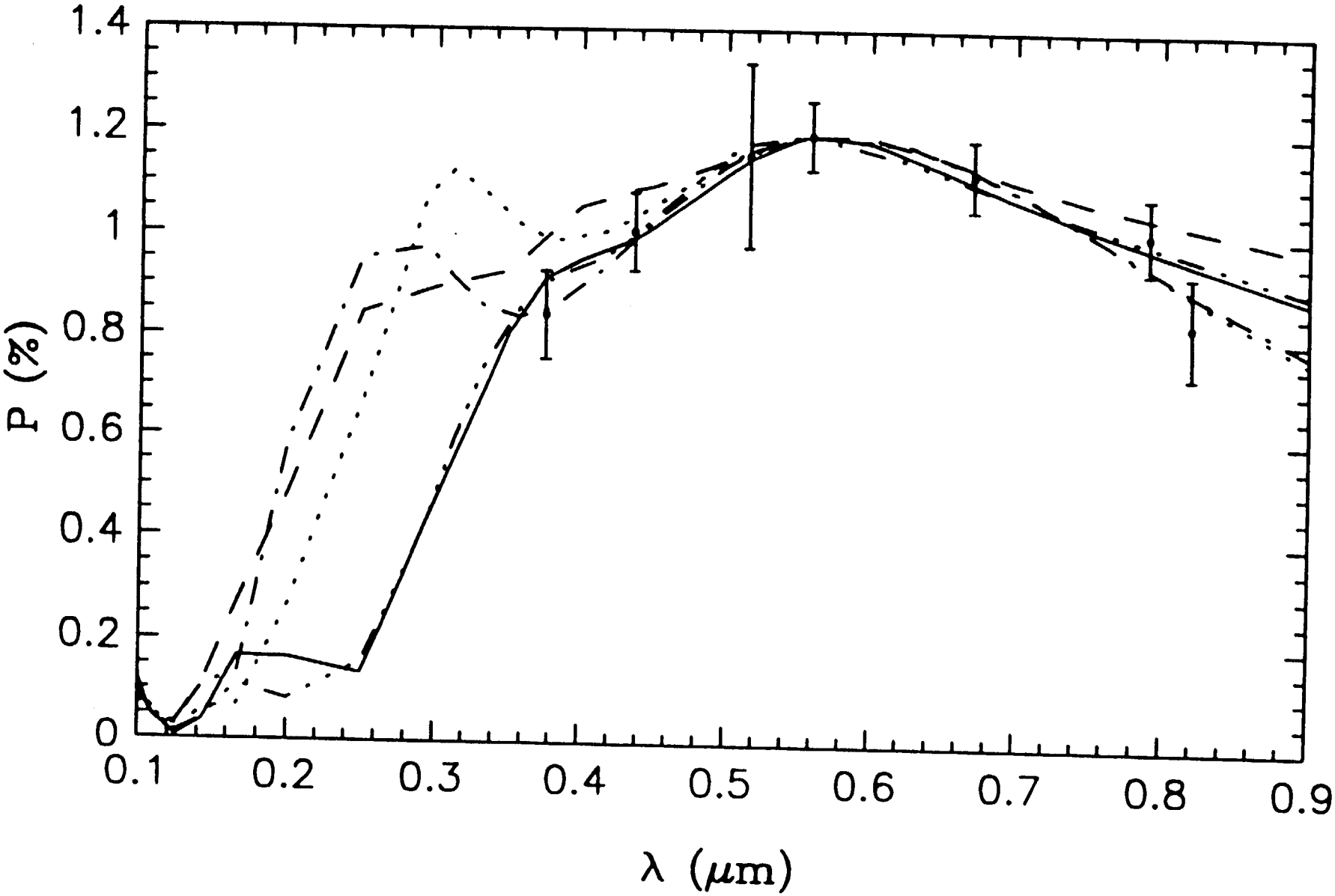

FIG. 10

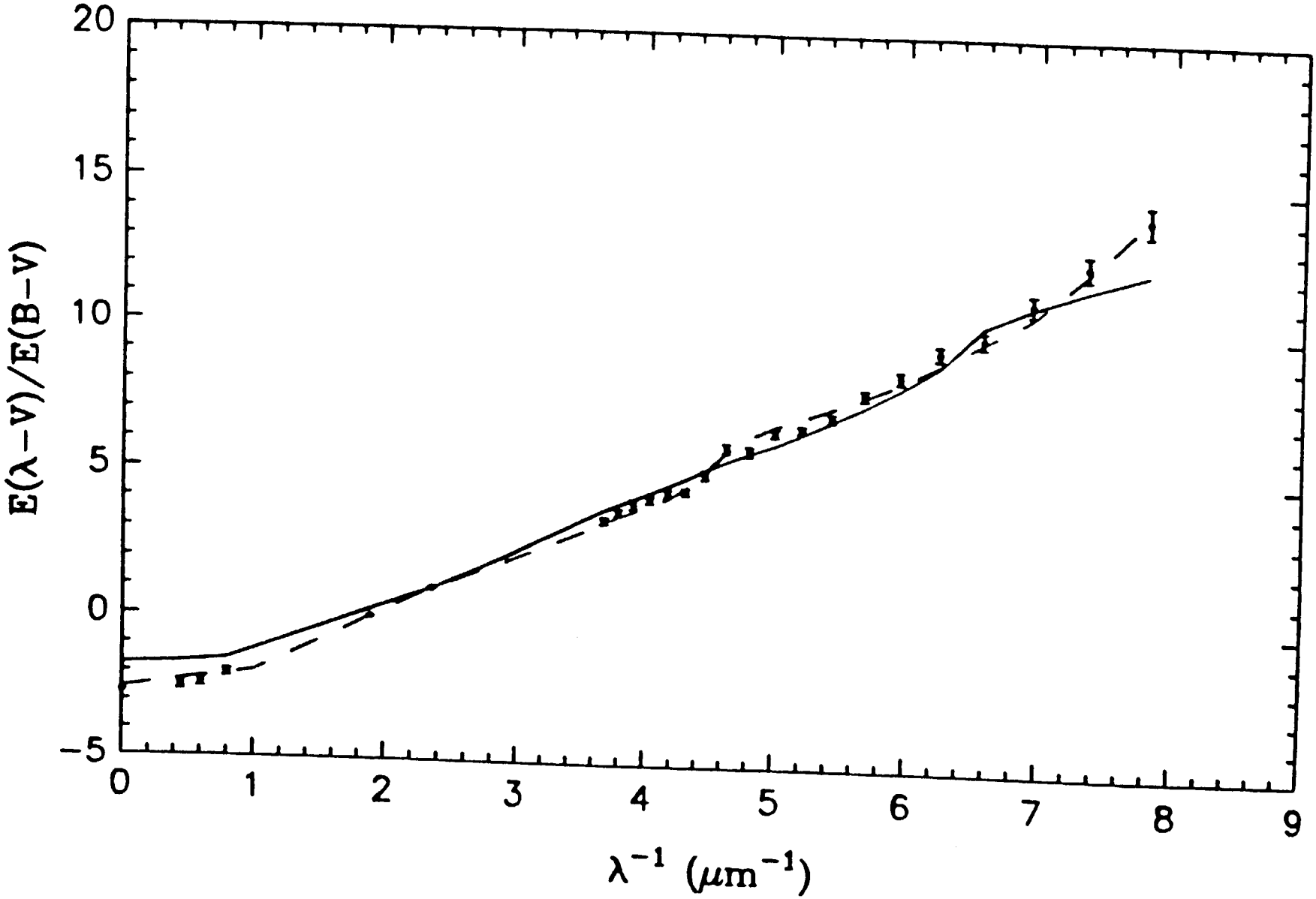

FIG. 11

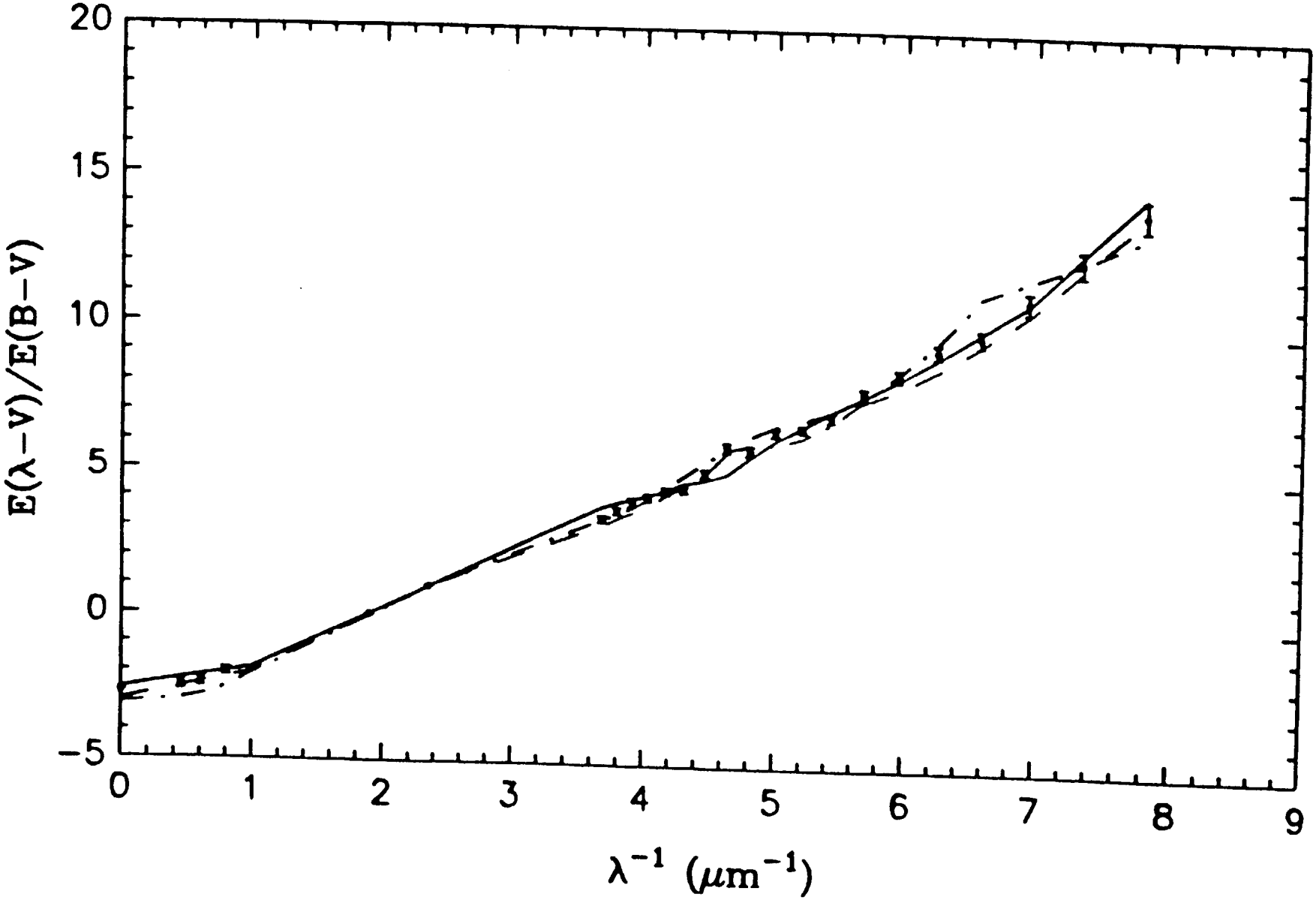

FIG. 12

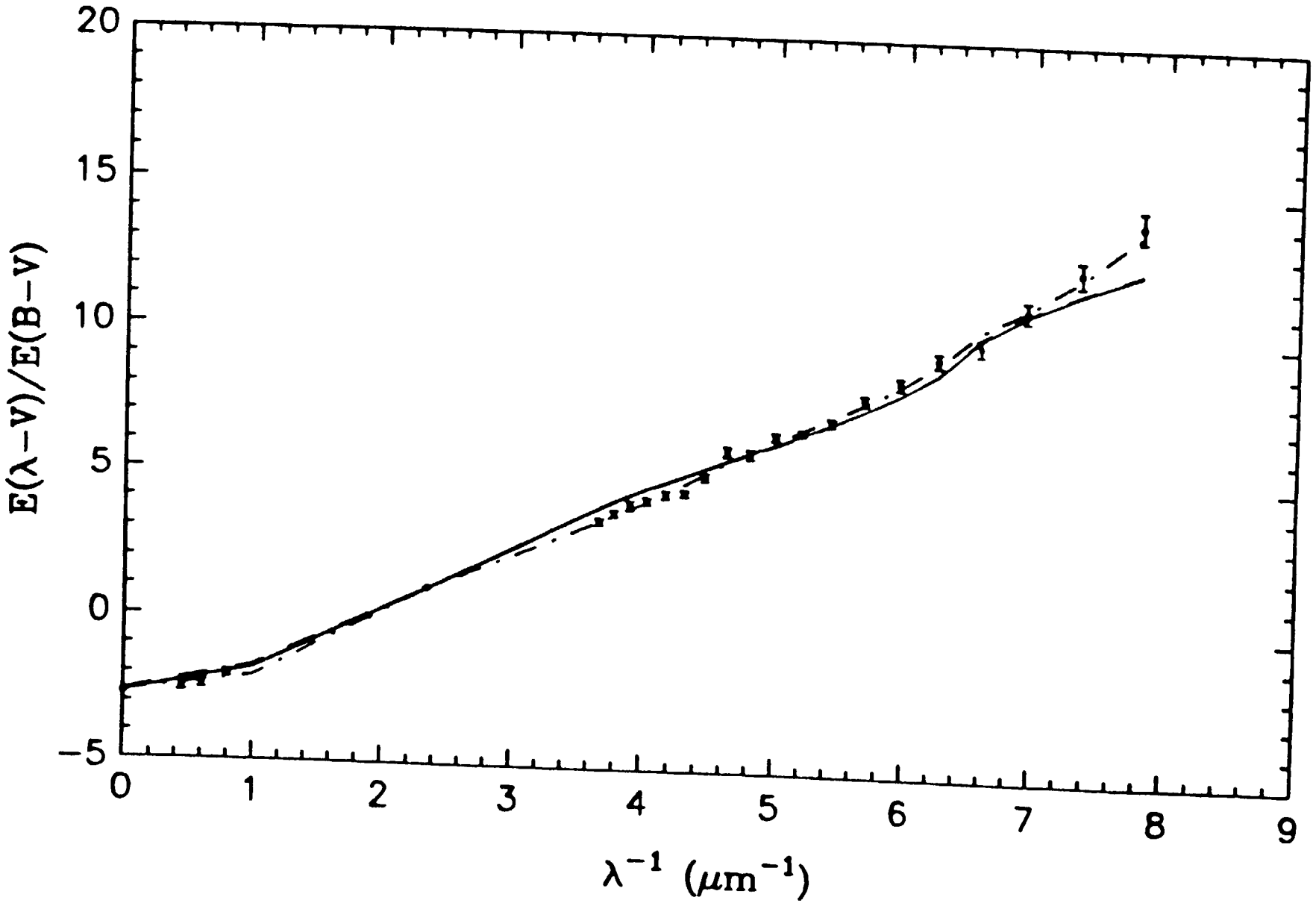

FIG 13

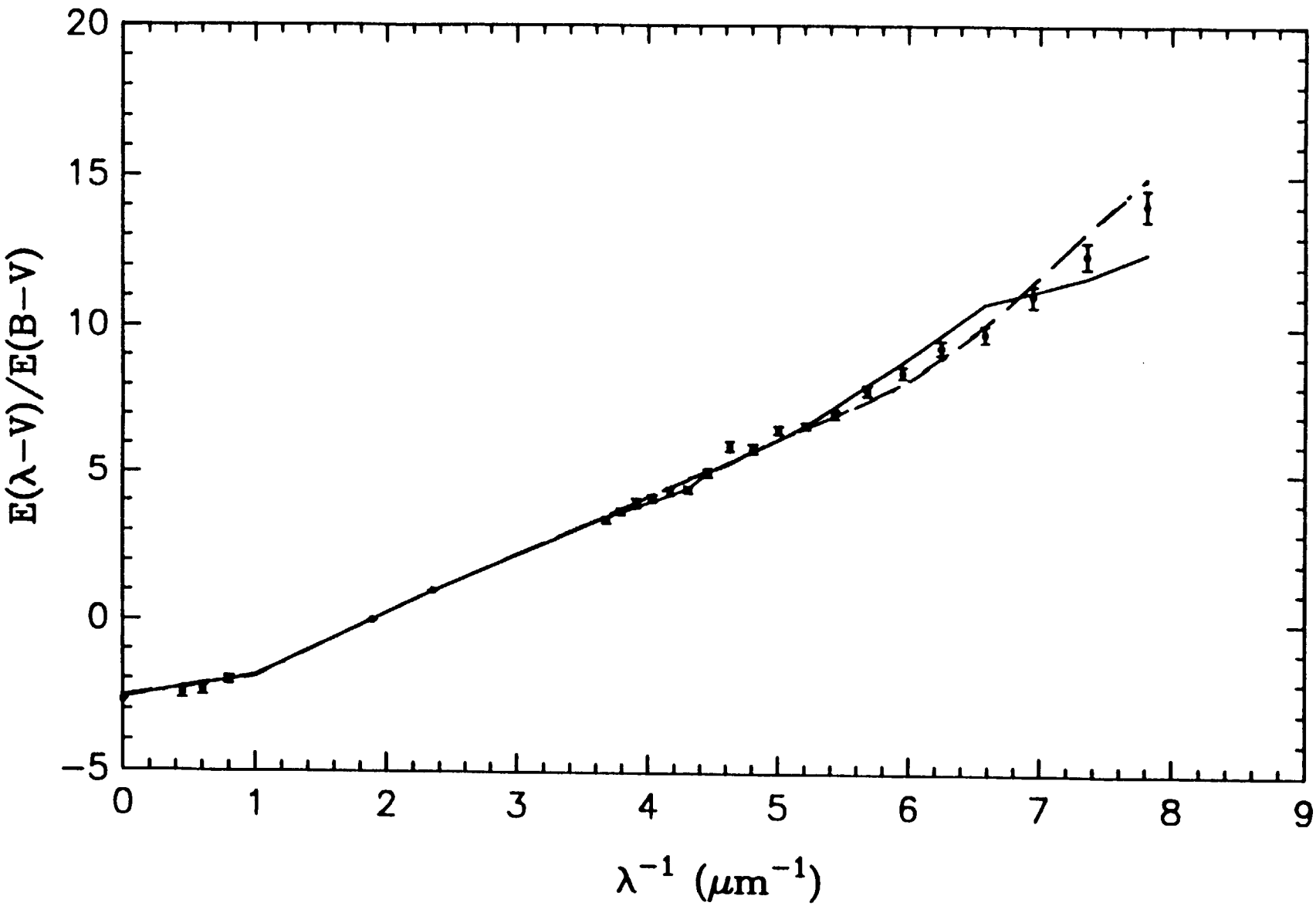

Fig. 14

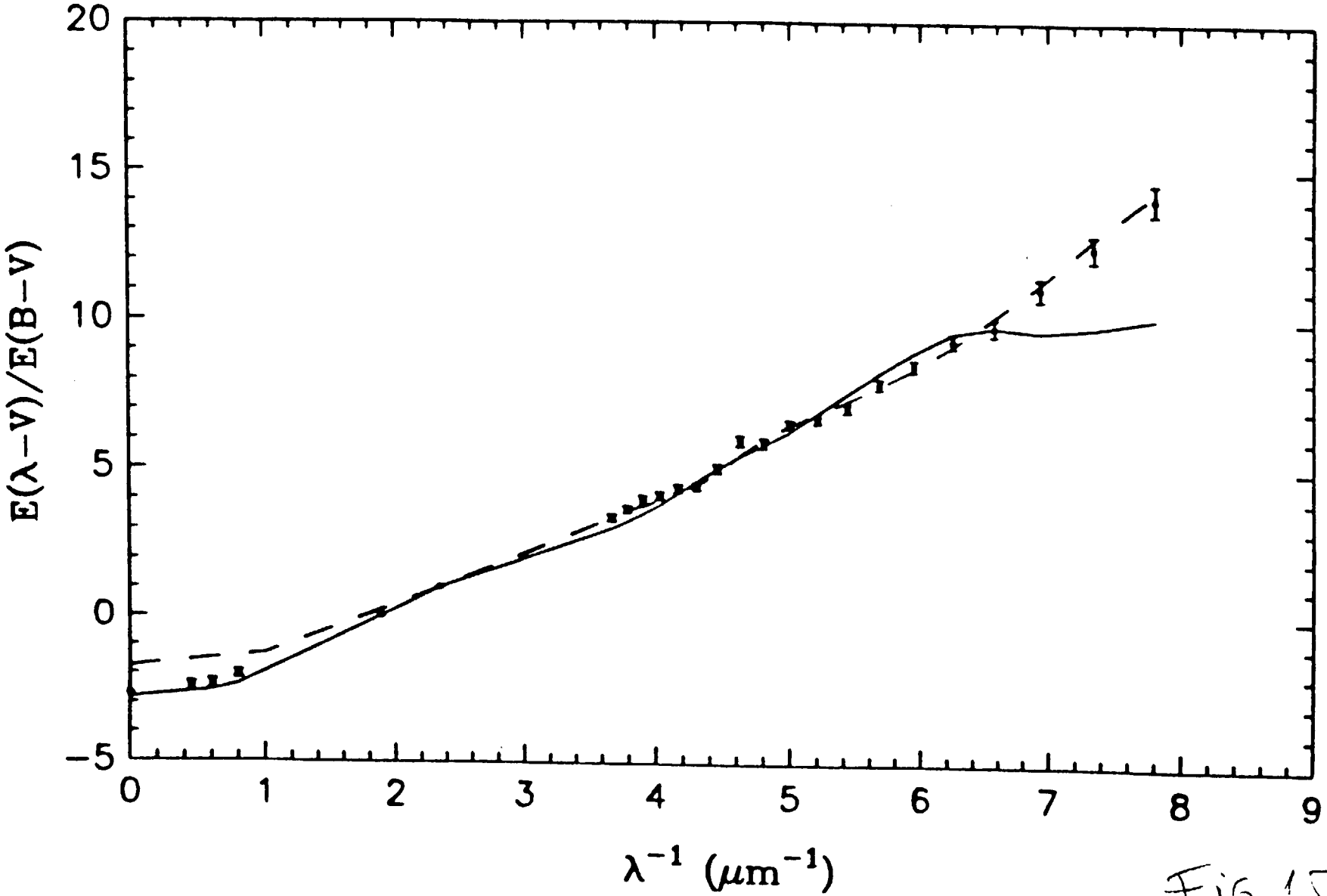

Fig. 15

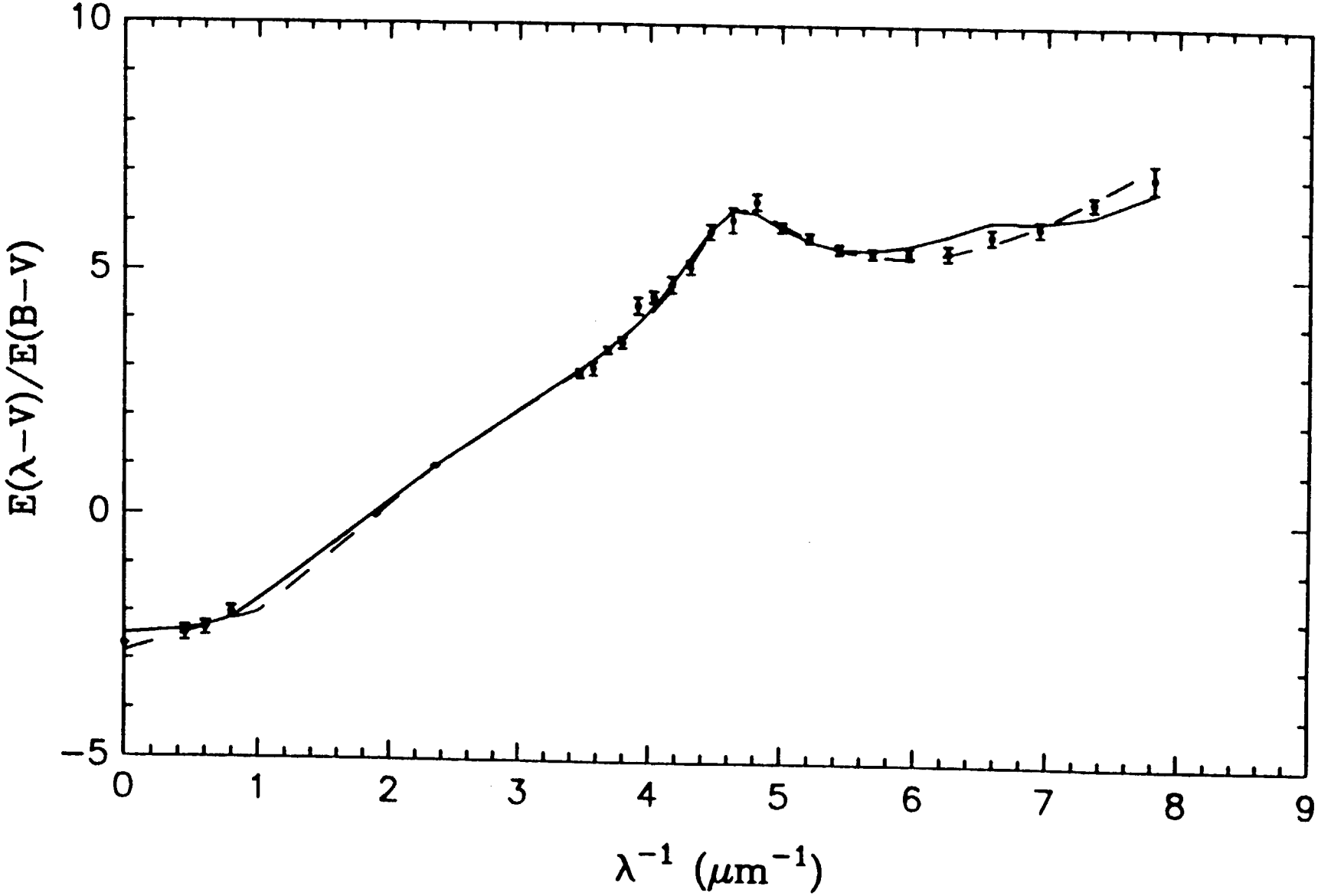

Fig. 16

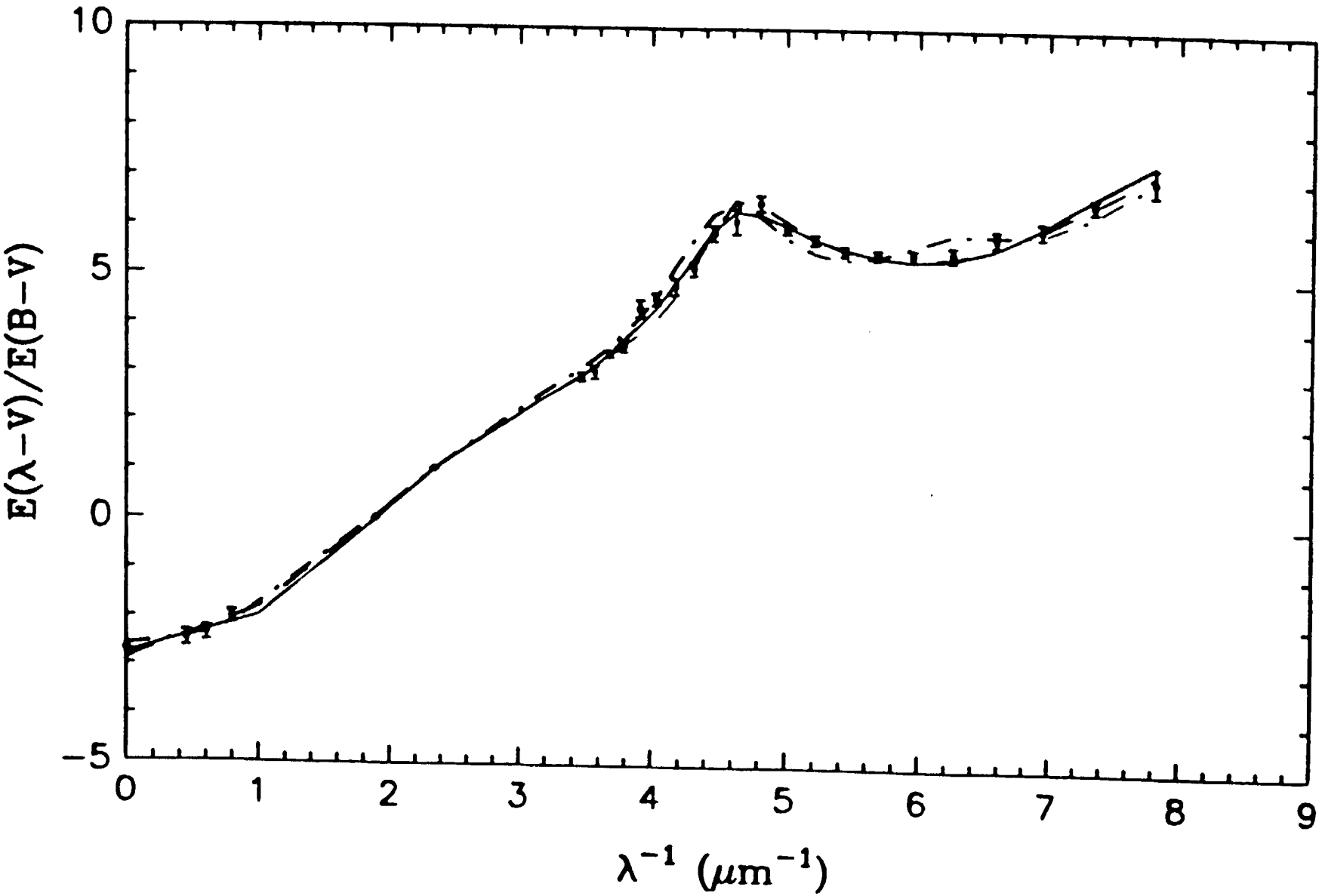

Fig. 17

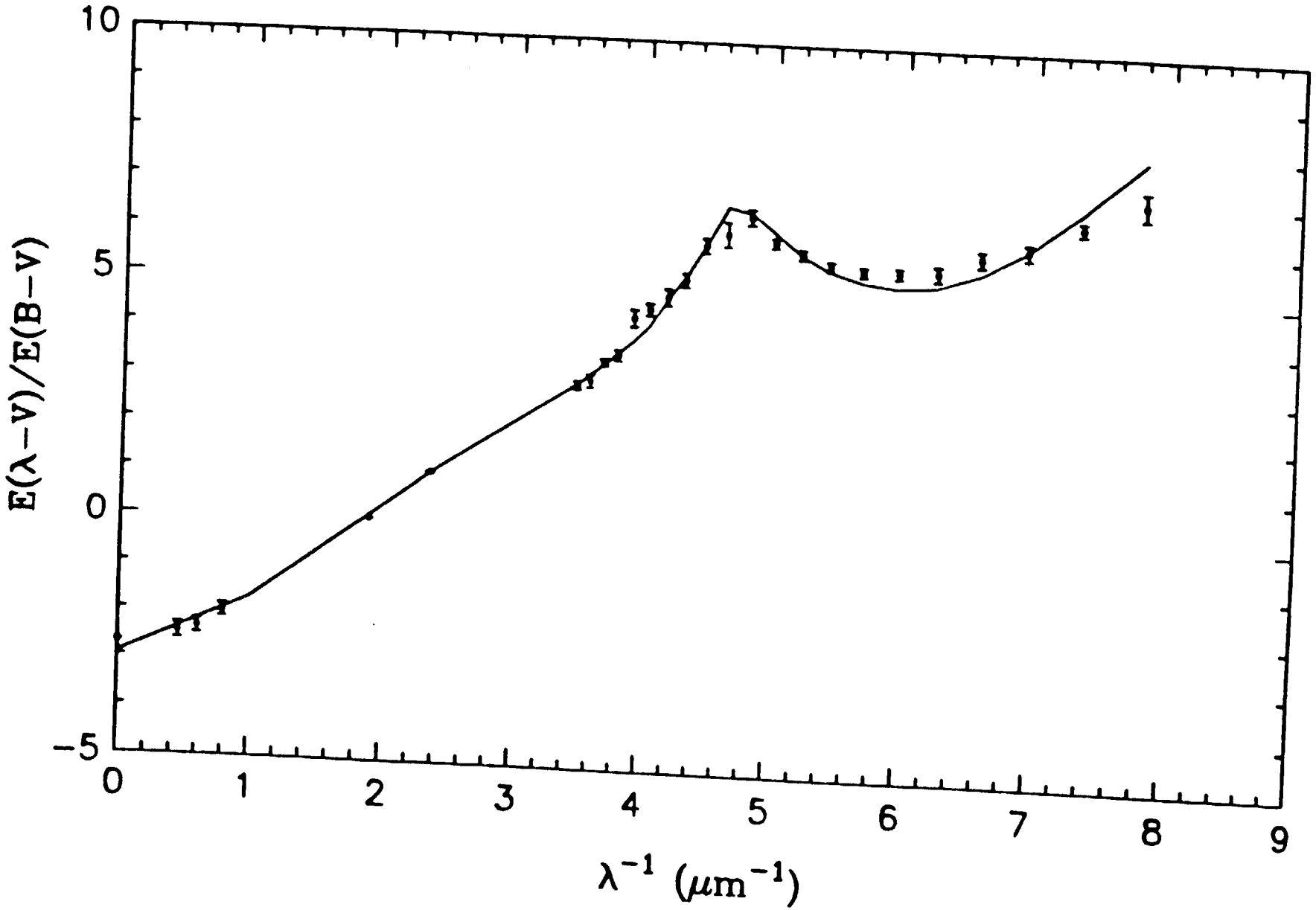

Fig. 18